



Strong disorder fixed points in the two-dimensional random-bond Ising model

Marco Picco, Andreas Honecker, Pierre Pujol

► To cite this version:

Marco Picco, Andreas Honecker, Pierre Pujol. Strong disorder fixed points in the two-dimensional random-bond Ising model. Journal of Statistical Mechanics: Theory and Experiment, IOP Science, 2006, pp.P09006. <10.1088/1742-5468/2006/09/P09006>. <hal-00079515v2>

HAL Id: hal-00079515

<https://hal.archives-ouvertes.fr/hal-00079515v2>

Submitted on 25 Aug 2006

HAL is a multi-disciplinary open access archive for the deposit and dissemination of scientific research documents, whether they are published or not. The documents may come from teaching and research institutions in France or abroad, or from public or private research centers.

L'archive ouverte pluridisciplinaire **HAL**, est destinée au dépôt et à la diffusion de documents scientifiques de niveau recherche, publiés ou non, émanant des établissements d'enseignement et de recherche français ou étrangers, des laboratoires publics ou privés.

Strong disorder fixed points in the two-dimensional random-bond Ising model

M. Picco¹, A. Honecker² and P. Pujol³

¹ *LPTHE*, Université Pierre et Marie Curie-Paris6 and
Université Denis Diderot-Paris7
Boîte 126, Tour 24-25, 5 ème étage,
4 place Jussieu, F-75252 Paris CEDEX 05, France,
e-mail: picco@lpthe.jussieu.fr.*

² *Institut für Theoretische Physik, TU Braunschweig,
Mendelssohnstr. 3, 38106 Braunschweig, Germany, and
Institut für Theoretische Physik, Universität Göttingen,
Friedrich-Hund-Platz 1, 37077 Göttingen, Germany,
e-mail: a.honecker@tu-bs.de.*

³ *Laboratoire de Physique[‡], ENS Lyon,
46 Allée d'Italie, 69364 Lyon Cédex 07, France,
e-mail: Pierre.pujol@ens-lyon.fr.*

(Dated: June 10, 2006)

ABSTRACT

The random-bond Ising model on the square lattice has several disordered critical points, depending on the probability distribution of the bonds. There are a finite-temperature multicritical point, called Nishimori point, and a zero-temperature fixed point, for both a binary distribution where the coupling constants take the values $\pm J$ and a Gaussian disorder distribution. Inclusion of dilution in the $\pm J$ distribution ($J = 0$ for some bonds) gives rise to another zero-temperature fixed point which can be identified with percolation in the non-frustrated case ($J \geq 0$). We study these fixed points using numerical (transfer matrix) methods. We determine the location, critical exponents, and central charge of the different fixed points and study the spin-spin correlation functions. Our main findings are the following: (1) We confirm that the Nishimori point is universal with respect to the type of disorder, *i.e.* we obtain the same central charge and critical exponents for the $\pm J$ and Gaussian distributions of disorder. (2) The Nishimori point, the zero-temperature fixed point for the $\pm J$ and Gaussian distributions of disorder, and the percolation point in the diluted case all belong to mutually distinct universality classes. (3) The paramagnetic phase is re-entrant below the Nishimori point, *i.e.* the zero-temperature fixed points are not located exactly below the Nishimori point, neither for the $\pm J$ distribution, nor for the Gaussian distribution.

PACS numbers: 75.50.Lk, 05.50.+q, 64.60.Fr

*Unité mixte de recherche du CNRS UMR 7589.

‡Unité mixte de recherche du CNRS UMR 5672 associée à l'Ecole Normale Supérieure de Lyon.

1 Introduction

The problem of disordered magnetic systems has attracted great interest in the past years and many questions still remain unanswered. An interesting problem is the universality class of second order phase transitions in two-dimensional systems. The random-bond Ising model (RBIM) is one of the simplest and best known of these systems [1, 2, 3, 4], but exhibits rich enough behaviour to give a general understanding of the problem. Further interest in the RBIM stems from analogies with the quantum Hall transition [5, 6, 7, 8] and applications in coding theory [9, 10, 11, 12].

For a small amount of randomness, the universality class of the RBIM remains unchanged, presenting only logarithmic corrections in some correlation functions [1]. For some particular kind of randomness, namely dilution, one can show that another non-trivial fixed point corresponds to a percolation universality class at zero temperature, since it becomes a purely geometric problem of having a thermodynamic number of spins within the same cluster. It is important to notice that in this case, all the randomly distributed bonds are non-negative.

The situation is quite different if some negative bonds are allowed in the probability distribution. For certain distributions with negative bonds, Nishimori [2, 3] has shown that some exact statements can be made about physical quantities. There is in particular a line in which the internal energy can be calculated exactly, known as the Nishimori line. The interest of this line goes further, since it has been shown that this line is invariant under renormalization group (RG) transformations [4]. Since this line crosses the ferromagnetic to paramagnetic transition line, the intersection point, known as the Nishimori point is a fixed point. Examples of probability distributions satisfying the Nishimori condition are the Gaussian, $\pm J$ binary and $0, \pm J$ with appropriately chosen weights (see below). Despite recent analytical approaches [6], the exact characterization of the universality class of this non-perturbative fixed point is still unknown. The underlying field theory describing this point is certainly a good representative of the disordered fixed-point behaviour with very interesting and rich phenomenology [13, 14]. In a previous letter [15], we have studied numerically the critical exponents and central charge of the Nishimori point in the $\pm J$ RBIM. We found in particular that its universality class does not correspond to the one of percolation, as one could have imagined in view of earlier numerical investigations of this model [16, 17, 18]. This is derived, first, from numerical estimates for the critical exponents and central charge which differ significantly from those of percolation, and confirmed by an analysis of higher moments of the correlation functions (which are all equal in percolation and only in pairs for the Nishimori point, see [15] for details and later in this paper).

The conclusion of a different universality class was confirmed in another numerical analysis by Merz and Chalker [19]. Thanks to a mapping to a network model, these authors reached big lattice sizes and high accuracy in the measurement of critical exponents. An interesting remark made by these authors concerns the dual theory of the RBIM¹, in which the different moments of the disorder field acquire negative dimensions [20]. More recently, Nishimori and Nemoto [21] used a generalized model with self-duality, and conjectured that the projection onto the RBIM gives the phase boundary for this

¹Because of the randomness introduced in the bonds, the model is not self-dual as the pure Ising model.

p_c	Method	Reference
Nishimori point in the $\pm J$ model		
0.111 ± 0.002	Transfer matrix	[30]
0.114 ± 0.003	Series expansion	[17]
0.1128 ± 0.0008	Non-equilibrium	[31]
0.1095 ± 0.0005	Transfer matrix	[18]
0.1094 ± 0.0002	Transfer matrix	[15]
0.1093 ± 0.0002	Fermionic transfer matrix	[19]
0.110028	Duality	[21]
≤ 0.178203	Rigorous upper bound	[32]
$T = 0$ critical point in the $\pm J$ model		
~ 0.099	Series expansion	[22]
0.105 ± 0.01	Matching algorithm	[23]
$0.095 < p_c < 0.108$	Matching algorithm	[24]
0.104 ± 0.001	Exact ground states	[25]
0.106 ± 0.002		
0.115	Ground state enumeration	[27]
0.1031 ± 0.0001	Exact ground states	[12]
0.103 ± 0.001	Exact ground states	[28]

Table 1: Overview of estimates for p_c at fixed points in the two-dimensional $\pm J$ random-bond Ising model. The first part of this table is for the Nishimori point, the second part for the zero-temperature critical point.

model. This result permits in particular to locate the Nishimori point analytically. The conjectured location is however outside the accuracy range of the most recent numerical works on the $\pm J$ binary disorder case [15, 19] and the validity of this conjecture is certainly a very interesting open issue.

The pure and the Nishimori point, when present in the phase diagram, are not the only non-trivial fixed points of the model: there is in any case a zero-temperature fixed point. While Nishimori’s results state rigorously that this point cannot be located at a higher concentration of “impure” bonds, analytical and numerical works on the $\pm J$ model [22, 23, 24, 12, 28, 25, 26, 27] tend to conclude that it is located at a smaller density of impurities, indicating a re-entrance of the ferromagnetic phase. The properties of the zero-temperature point vary considerably with the kind of disorder introduced. For a symmetric Gaussian distribution, it has been shown [29] that the lowest energy configuration is unique (modulo the \mathbb{Z}_2 symmetry) with probability one. One is tempted to check the extension of this result to our zero-temperature point, and check for example that, for a given configuration of the disorder, any spin-spin correlation function is 1 or -1 . Then, all the odd moments of the spin-spin correlation functions are equal, and all the even moments are just equal to 1, a result that is similar, but not exactly identical to the percolation case. The situation is much more subtle for distributions like the $\pm J$ one, since frustration plays a crucial role. For a generic configuration of disorder, the lowest energy states are expected to be highly degenerate. The results obtained by different techniques for the location of both, the Nishimori point and the zero-temperature critical point are summarized in Table 1 for the $\pm J$ model. As can be seen from the most recent results, the zero-temperature critical point seems to be located at a concentration

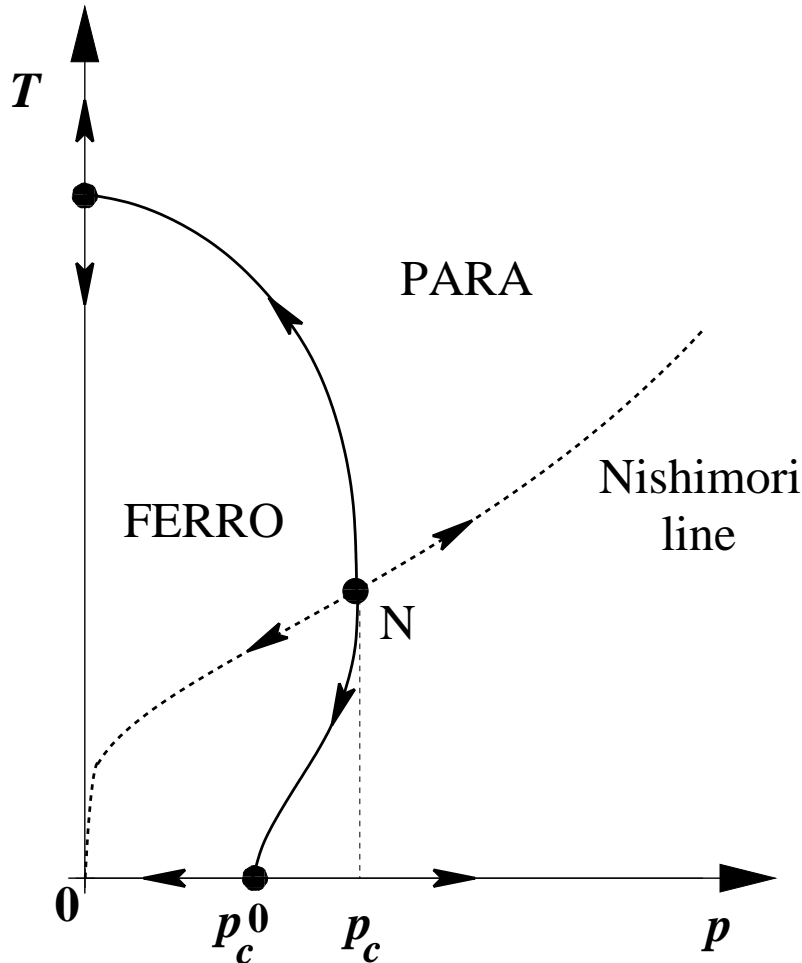


Figure 1: Phase diagram of the two-dimensional $\pm J$ random-bond Ising model. The arrows represent the flow under the renormalization group.

of “impure” bonds strictly smaller than the one of the Nishimori point. A schematic picture of the phase diagram of the $\pm J$ case in the $p - T$ plane (p being the number of antiferromagnetic bonds) is shown in Fig. 1, where the separation of the paramagnetic and ferromagnetic phases, as well as the Nishimori line are drawn. The location of the Nishimori point N and the zero-temperature critical point are representative of the results shown in Table 1. For the case of the Gaussian disorder, a similar diagram may be obtained by replacing the parameter p with the variance of the distribution of disorder, σ , although the shape of the Nishimori line is different.

Given a simple phase diagram as shown in Fig. 1, it is tempting to trace the massless flow backwards from the pure Ising model at $p = 0$ to the Nishimori point N [33, 34]. However, we will argue in this paper that in a generalized parameter space there are in fact several fixed points on the massless surface with different universality classes such that a backtracking procedure is in general ambiguous. Indeed, the problems encountered in [34] were one of the original motivations for our earlier numerical study of the Nishimori point [15] which we continue and expand here.

In this paper we provide an extensive numerical analysis of the random-bond Ising model for three different kinds of probability distributions. We first consider in parallel

the case of Gaussian and $\pm J$ distributions for which we estimate the location of the fixed point along the Nishimori line using domain-wall techniques. We compute the free energy with a transfer matrix technique [35] and obtain the central charge by analyzing the finite-size corrections. We also compute the spin-spin correlation functions on long strips to obtain the magnetic exponent. This and other measurements to check consistency clearly show that the models with $\pm J$ and Gaussian distributions share the same universality class at their respective Nishimori points. The compatibility of the results between the $\pm J$ and Gaussian cases further elucidates the nature of the universality class of this point which was recently argued to be different from the one of percolation [15, 19]. We next consider dilution, which can be modeled by a probability distribution allowing the values of $\pm J$ and 0 for the coupling constants. In the case of pure dilution (allowing only values $+J$ and 0 for the coupling constants), the other fixed point apart the one of the pure model is located at zero temperature and dilution $q_c = 1/2$ and simply corresponds to bond percolation. The $\pm J, 0$ distribution allows us to study the behaviour in the critical line between the Nishimori point and the percolation point. In particular, by studying the value of the effective central charge for different strip widths and its evolution towards larger sizes we show that the percolation fixed point is repulsive along this critical line in favour of the Nishimori point. The same technique is used to confirm that the Nishimori point is unstable with respect to the pure Ising fixed point when moving on the critical line connecting these two points. We finally address the problem of the zero-temperature fixed point. Although for the case of the $\pm J$ distribution there is an extensive list of numerical works indicating re-entrance of the ferromagnetic phase (see Table 1), to our knowledge there was no conclusive evidence of the same fact for the Gaussian distribution. We show here clear evidence for the re-entrance of the phase also for the Gaussian distribution. We compute also different moments of spin-spin correlation functions and the magnetic exponent. Our results in the magnetic sector clearly show that the universality class of this zero-temperature critical point is once again different from the one of the finite-temperature Nishimori point as well as percolation, in contrast to what one could have thought considering previous numerical results in two dimensions [17, 25].

2 Some definitions

In this section, we present some definitions which will be used throughout this paper. We will consider two kinds of probability distributions $P(J)$ for the bonds: a discrete distribution where the coupling constants can take values ± 1 and 0, and a continuous Gaussian distribution. In the case of a discrete distribution, two subclasses can be considered, the first one allows only the values ± 1 while the second and more general one, allows also the value 0 for the coupling constants. This last case corresponds to dilution. In any case we can imagine a phase diagram in which the vertical axis is given by temperature and the horizontal axis by a parameter representing the strength of the disorder (see Figure 1).

Let us define the Hamiltonian of the two-dimensional Ising model to be:

$$H = - \sum_{\langle i,j \rangle} J_{i,j} \delta_{S(i),S(j)} , \quad (2.1)$$

where $S(i) = \pm 1$ and $\langle i, j \rangle$ means nearest neighbours on a square lattice. The variables

$J_{i,j}$ are random and independently chosen with a probability distribution function $P(J)$. As usual, the Kronecker delta function is zero if the spins are different and one if they are equal. To establish the relation to other conventions for the energy note that it can be expressed in terms of products of Ising spins via $\delta_{S(i),S(j)} = (S(i)S(j) + 1)/2$.

The Nishimori line is defined by the condition [2]:

$$P(-J) = \exp(-\beta J) P(J), \quad (2.2)$$

where $\beta = \frac{1}{k_B T}$ is the inverse temperature (from now on we choose the convention $k_B = 1$). Let us analyze the Nishimori condition for the different distributions considered here

- $J = \pm 1$: The distribution is characterized by the concentration of antiferromagnetic bonds p :

$$P(J) = (1 - p) \delta(J - 1) + p \delta(J + 1). \quad (2.3)$$

Eq. (2.2) gives the following condition for the Nishimori line

$$\beta = \ln \left(\frac{1 - p}{p} \right), \quad (2.4)$$

which is schematically depicted in Fig. 1. The line extends from the (attractive) fixed points given by $T = 0, p = 0$ and $T = \infty, p = 1/2$ and crosses the Para-Ferro transition line at the critical concentration p_c . In the first part of Table 1 we summarize estimates for the location of the critical point p_c . With the exception of a conjectured duality property [21] and a rigorous upper bound [32], all the other results come from numerical simulations.

- Gaussian distribution:

$$P(J) = \sqrt{\frac{1}{2\pi\sigma^2}} \exp \left(-\frac{(J - J_0)^2}{2\sigma^2} \right), \quad (2.5)$$

with the following condition

$$\beta = \frac{J_0}{\sigma^2} \quad (2.6)$$

for the Nishimori line. In the following, we will choose $J_0 = 1$ without any loss of generality. Thus, the distribution is characterized by the parameter σ along the Nishimori line which extends from the (attractive) fixed points given by $T = 0, \sigma = 0$ and $T = \infty, \sigma = \infty$ and crosses the Para-Ferro transition line at the value σ_c . The first numerical characterization of the critical point was given in [16], with a value of $\sigma_c \sim 0.97$.

- Finally, the binary distribution can be generalized to include dilution. In this case, we write:

$$P(J) = q \delta(J) + (1 - q - p) \delta(J - 1) + p \delta(J + 1). \quad (2.7)$$

The case $q = 0$ corresponds to the binary distribution discussed above, while $p = 0$ gives the ferromagnetic diluted model. In the diluted model there is only a fixed point located at zero temperature and $q_c = 1/2$, apart from the pure model fixed point [36]. This $T = 0$ fixed point corresponds to percolation. The reason

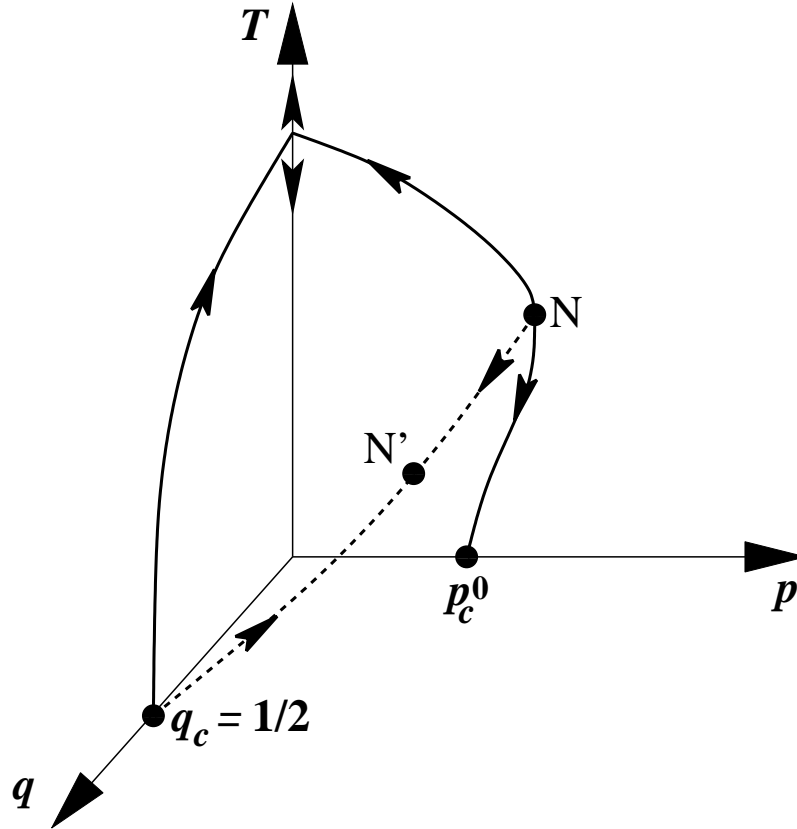


Figure 2: Phase diagram of the diluted $\pm J, 0$ random-bond Ising model. p and q are the concentration of negative and zero bonds, respectively. The arrows represent the flow under the renormalization group. The dashed line represents the intersection between the Nishimori surface and the Ferro-Para transition surface.

for this is that in the absence of frustration all the spins belonging to the same cluster must point to the same direction at zero temperature. Then, whenever there is percolation, or a cluster containing a macroscopic number of spins, there is a macroscopic magnetization, and this happens until the critical concentration of bonds $1/2$ (see for example [36, 37]).

The Nishimori surface in the T - p - q space is now given by:

$$\beta = \ln \left(\frac{1 - p - q}{p} \right). \quad (2.8)$$

The intersection of this surface with the ferromagnetic-paramagnetic transition surface gives a renormalization group invariant line [4] whose end points are the percolation $q = 1/2$, $T = 0$ fixed point and the finite-temperature Nishimori point N of the purely binary case as depicted in Fig. 1. In the $T - p - q$ phase diagram, the location of the Nishimori point, here called N', must be within the intersection line mentioned above (the dashed line in Fig. 2). In this sense, the point N depicted in Fig. 1 is the representative in the $T - p$ space of the more general location of the Nishimori point denoted by N' in Fig. 2.

3 Domain-wall free energy

In the following section we will discuss the domain-wall free energy in a manner very similar to [16]. For a strip of width L the domain-wall free energy d_L is defined as

$$d_L = L^2 \left(f_L^{(p)} - f_L^{(a)} \right), \quad (3.1)$$

where $f_L^{(p)}$ is the free energy *per site* $f_L^{(p)} = \frac{\ln Z^{(p)}}{LM}$ of a strip of width L and length M with *periodic* boundary conditions² and $f_L^{(a)} = \frac{\ln Z^{(a)}}{LM}$ the corresponding one with *antiperiodic* boundary conditions.

d_L measures the free energy associated to a domain wall in the system. We will first consider the $\pm J$ distribution of disorder. For fixed parameters p (β) in the disordered (paramagnetic) phase, one should have $\lim_{L \rightarrow \infty} d_L \rightarrow 0$ while d_L should diverge in the ordered phase ($d_L \rightarrow \infty$ as $L \rightarrow \infty$). At the fixed point p_c (β_c), d_L should converge quickly with L . We can therefore use crossing points between d_{L_1} and d_{L_2} to obtain finite-size estimates for p_c .

Let us consider first the $\pm J$ distribution of disorder. $f_L^{(p)}$ and $f_L^{(a)}$ are computed with the transfer matrix technique (see, e.g., [35]) on strips of length 10^6 . Averages over up to $N \approx 4000$ samples of such $L \times 10^6$ strips are taken in order to average over randomness and to determine the statistical error. It is useful to fix the number of bonds on each $L \times 10^6$ strip to approximate the chosen value of p as accurately as possible: In our implementation such a strip has $L \cdot (2 \cdot 10^6 - 1)$ bonds out of which we select the integer closest to $p L \cdot (2 \cdot 10^6 - 1)$. We found that this method leads to 5 times smaller error bars for $f_L^{(p)}$ than if one selects each bond *separately* at random with probability p , *i.e.* for the same precision one needs 25 times less samples with this method compared to generating

²Note that our sign conventions differ from the standard ones.

each bond at random with probability p without constraining their total number. For d_L the improvement is even bigger and the error bars become 10 times smaller – or one needs 100 times less samples for the the same accuracy.

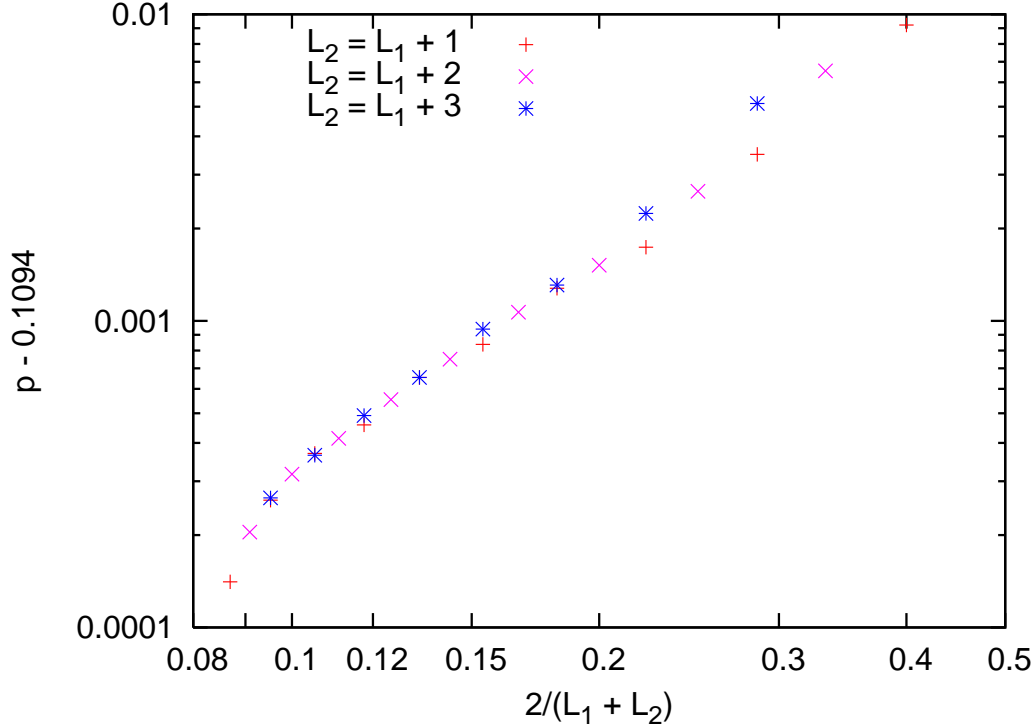


Figure 3: Position p of crossings between $d_{L_1}(p)$ and $d_{L_2}(p)$ on the Nishimori line of the $\pm J$ random-bond Ising model with $L_2 \leq 12$.

Next we will present some details of the analysis leading to the results presented in [15] – a very similar computation was also performed in [19]. Fig. 3 shows a doubly logarithmic plot of the crossing point $p_c(L_1, L_2)$ between $d_{L_1}(p)$ and $d_{L_2}(p)$, using $p_c = 0.1094$ in the shift of the vertical axis. It is known for the pure Ising model that the finite-size corrections to p_c scale roughly $\sim L^{-2}$ with $L = (L_1 + L_2)/2$ [38]. In order to extrapolate p_c to the thermodynamic limit, one can therefore first use a plot of finite-size estimates for p_c as a function of L^{-2} and extrapolate to the vertical axis. A reasonable extrapolation with a generous error bar is

$$p_c = 0.1093 \pm 0.0004. \quad (3.2)$$

Even if the correction is probably not of the form $1/L^2$ in the present case, one can see in Fig. 3 that the finite-size correction to p_c is well described by a power in L . For an improved extrapolation we therefore use the following form for a fit:

$$p_c(L_1, L_2) = p_c + \alpha \left(\frac{L_1 + L_2}{2} \right)^{-\xi}. \quad (3.3)$$

We then find [15]

$$p_c = 0.1094 \pm 0.0002 \quad (3.4)$$

and an exponent

$$\xi = 1.5 \pm 0.3. \quad (3.5)$$

The two estimates (3.2) and (3.4) agree well with each other – the error bar of the second one is just a little smaller. The exponent (3.5) cannot be determined very accurately.

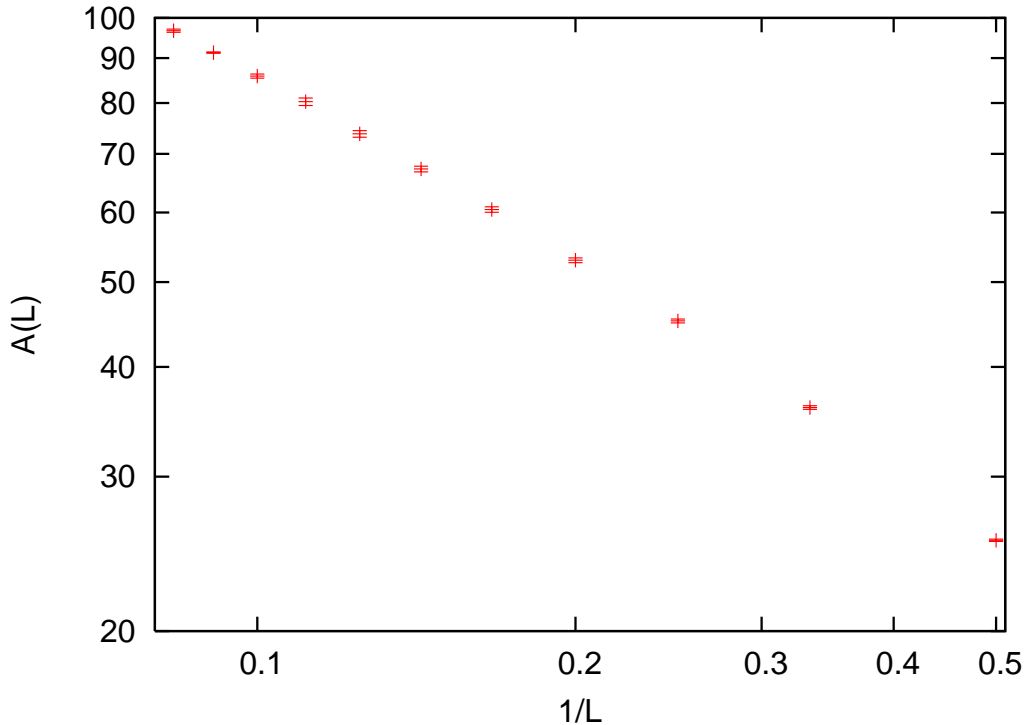


Figure 4: Slope $A(L)$ of the domain-wall free energy for the $\pm J$ random-bond Ising model as a function of $1/L$.

The estimates (3.2) and (3.4) should be compared with other estimates which are summarized in Table 1. At this point comparison with the zero-temperature transition is meaningful only if one assumes that the $T = 0$ transition point is located exactly below the Nishimori point. Our estimate agrees within error bars with other transfer matrix computations [30, 18, 19]. However, our estimate falls outside error bars of estimates obtained by other methods: It is smaller than the estimates of [17, 31] (in the latter case significantly). This discrepancy becomes clearest if one notices that several of our finite-size crossings have already reached the region $p \approx 0.1097$ (see also Fig. 2 of [15]). If one now assumes that these crossings decrease monotonically with increasing L (as the data in Fig. 3 indeed does), one does not need to actually carry out the extrapolation and estimate its error in order to conclude that our extrapolated value for p_c must end up below the error windows of [17, 31]. At this point it is particularly reassuring to observe that our result is fully consistent with the one of [19] which has been obtained using also substantially wider strips (up to $L = 64$). Furthermore, (3.4) is in complete agreement with other quantities to be discussed in later sections. Thus, we observe a significant difference between the analytic estimate of [21] obtained from a duality argument and our value for p_c as well as the one of Merz and Chalker [19].

Now let us look at a first critical exponent, namely the correlation length exponent ν along the Nishimori line. If one assumes the scaling form

$$d_L(p - p_c) = d((p - p_c)L^{1/\nu}) , \quad (3.6)$$

one can expand around p_c and finds

$$d_L(p - p_c) \sim \text{const.} - A(L)p \quad (3.7)$$

with

$$A(L) \sim L^{1/\nu} . \quad (3.8)$$

Then one can fit d_L close to p_c by a linear function and extract $A(L)$.

Fig. 4 shows the values for $A(L)$ determined in this manner on a doubly logarithmic scale³. One can see that they follow indeed a power law. Using (3.8) we extract

$$\nu = 1.48 \pm 0.03 , \quad (3.9)$$

which amounts to a slight correction of the value $\nu = 1.33 \pm 0.03$ obtained in [15]. The result (3.9) is now in excellent agreement with the value $\nu = 1.50 \pm 0.03$ obtained by a fermionic transfer matrix [19]. The most recent results $\nu \approx 1.5$ do no longer agree well with $\nu = 1.32 \pm 0.08$ obtained by high-temperature series [17]. However, we already observed above that the series expansion method does not yield a very accurate estimate for p_c either. Furthermore, the value $\nu = 4/3$ characteristic for percolation (see e.g. [37]) now falls outside numerical errors and thus it is possible to conclude that the Nishimori point is not in the universality class of percolation already on the basis of the exponent ν . Note that the result (3.9) does not involve locating p_c precisely and should therefore be independent of errors which may have been made in the location of p_c .

Figures with scaling collapses of d_L were presented in [15,39] with $\nu = 1.33$ and in [19] with $\nu = 1.50$. While they verify that d_L obeys indeed the scaling form (3.6), the fact that reasonable collapses can be obtained for different values shows that such a collapse is not a good criterion for determining ν .

We now present the same domain-wall free energy analysis for the Gaussian distribution of disorder. Again, $f_L^{(p)}$ and $f_L^{(a)}$ are computed with the transfer matrix technique for small sizes. For larger sizes ($L = 15, 18, 21, 24$), we employed a different algorithm, developed by Merz and Chalker, which uses a mapping to a network model, see [19] for details. For each point we averaged over 10 000 samples of size $L \times 10^6$. In Fig. 5, we show a plot of the crossing point $\sigma(L_1, L_2)$ between $d_{L_1}(\sigma)$ and $d_{L_2}(\sigma)$. Contrary to the $\pm J$ case where the crossing was converging quickly, here we see that the situation is much more complex. For the smaller sizes with $L_2 = L_1 + 2$ and $2/(L_1 + L_2) \geq 0.15$, it apparently converges to $\sigma \simeq 0.9815$. For larger sizes, we see a different behaviour. We explain this change of behaviour by the existence of an irrelevant operator. If such an operator exists, we expect that close to the critical point, the domain-wall free energy can be expanded as [16, 19, 38]:

$$d_L(\sigma) = a + b(\sigma - \sigma_c)L^{1/\nu} + cL^{-x} . \quad (3.10)$$

³Our data for d_L is in perfect agreement with that of [19] where we overlap. However, the windows in p used for the present estimates of $A(L)$ differ from those used in [15] leading to slightly different results.

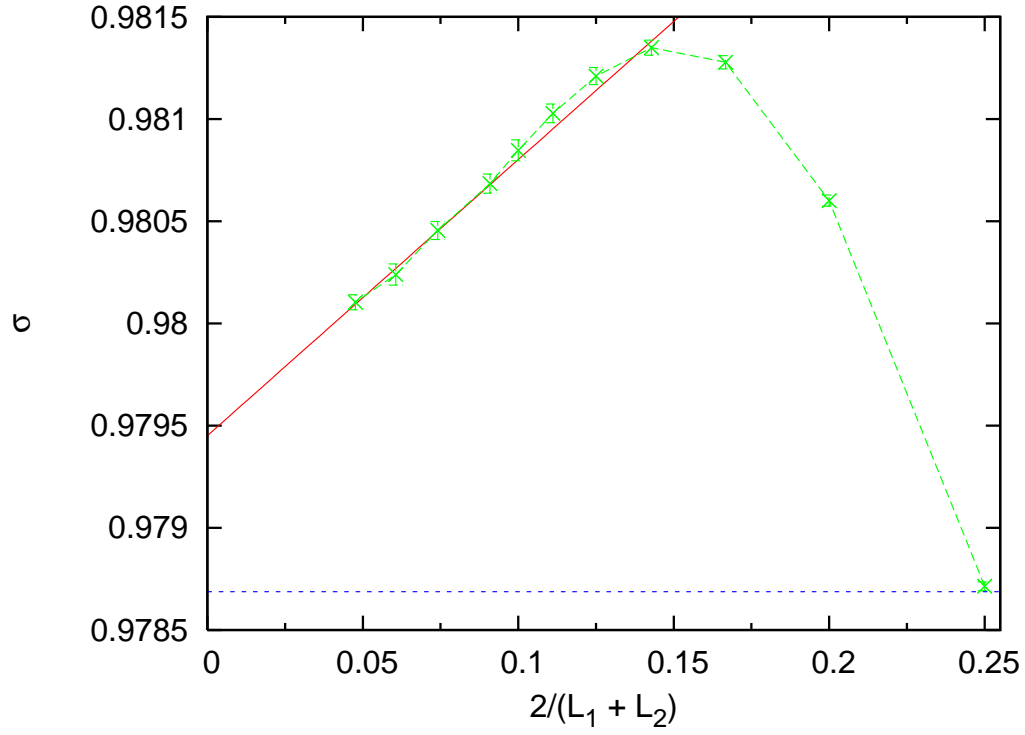


Figure 5: Position σ of crossings between $d_{L_1}(\sigma)$ and $d_{L_2}(\sigma)$ on the Nishimori line of the Gaussian random-bond Ising model. The figure also contains a linear fit to the large size data and the value $\sigma = 1/1.02177$ predicted by duality arguments [21].

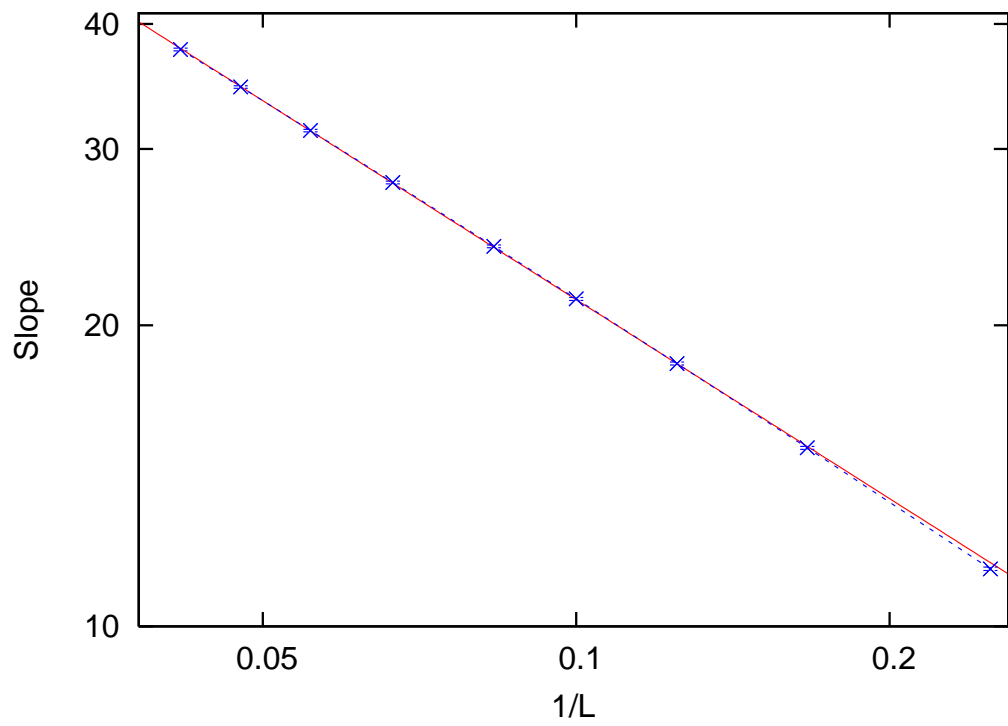


Figure 6: Slope of the domain-wall free energy of the Gaussian random-bond Ising model as a function of $1/L$.

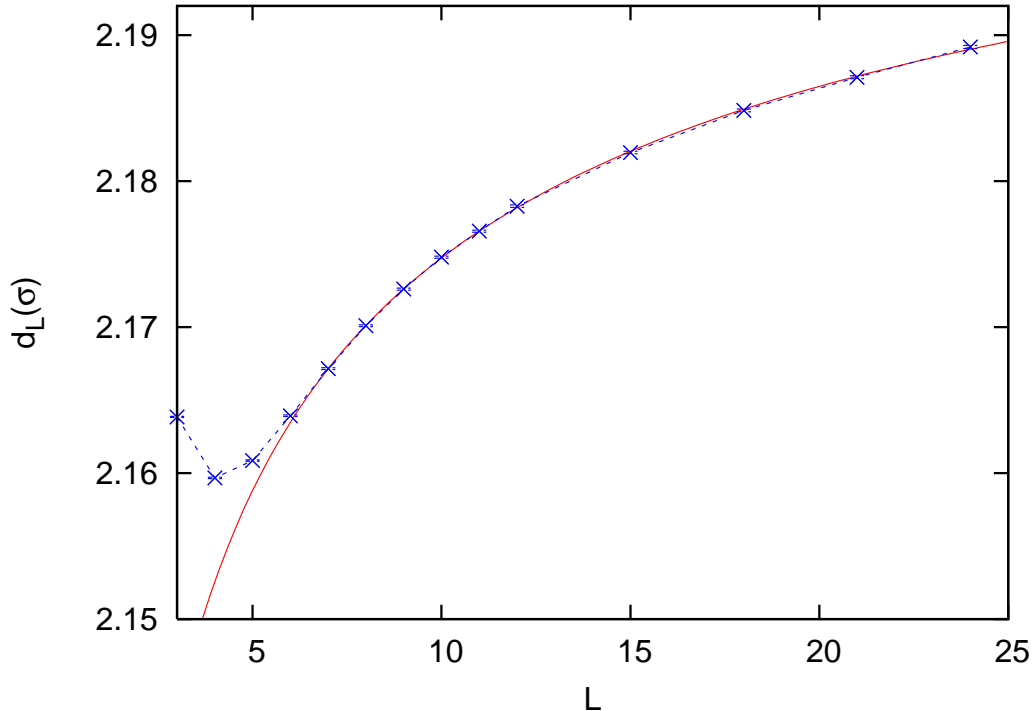


Figure 7: Domain-wall free energy of the Gaussian random-bond Ising model at $\sigma_c = 0.97945$ as a function of L . We also show a plot of the fit to the form (3.10) with $L \geq 7$.

Here we have neglected a further contribution coming from the thermal exponent ν_T (see [19]) which is sub-leading compared to the $(\sigma - \sigma_c)$ term. The last contribution corresponds to an irrelevant operator, of dimension $2 + x$, associated to the Nishimori point. In principle it should also be present in the scaling of the Nishimori point with the $\pm J$ distribution although much bigger sizes may be necessary for its observation. If we take only the points with $2/(L_1 + L_2) < 0.1$ then the data in Fig. 5 seems to converge linearly to a point that we determine by a fit to be

$$\sigma_c = 0.97945 \pm 0.00004. \quad (3.11)$$

In Fig. 5 we also show the plot corresponding to this linear fit (for the larger sizes) as well as the value $\sigma = 1/1.02177 = 0.978694$ predicted by duality arguments [21]. While the two values are close, they are still not compatible from our analysis. If one changes the parameters of the linear fit, allowing for smaller size data to be taken in account, the smallest possible value that we get is $\sigma = 0.97939 \pm 0.00002$ which is still not compatible with the duality argument value. The only other numerical estimate of σ_c that we are aware of is the one of McMillan [16], $\sigma_c \simeq 0.93 - 0.97$. This result is not expected to be highly accurate since it is obtained on small systems of linear sizes up to $L = 8$.

Next we turn to the determination of ν . Again, we compute it by looking at the slope of the domain-wall free energy close to the critical point. In Fig. 6, we show the slope as a function of the size. The slope is determined in the following way: for each size, we computed $d_L(\sigma)$ for $\sigma = 0.980$ and $\sigma = 0.982$. (For the sizes that we considered,

the effective critical value of $\sigma_c(L)$, determined as the crossing of the domain-wall free energies, is always in this range, see Fig. 5). Thus the slope is determined directly from the difference between these two values for each size. We also show in this figure the best fit to the form $\simeq L^{1/\nu}$. This fits perfectly the data for $L > 4$. We obtain $\nu = 1.52(3)$ which is very close to the result for the $\pm J$ disorder case. Note that using a transfer matrix method McMillan [16] obtained $\nu \approx 1.58$ for the Gaussian random-bond Ising model.

In Fig. 7, we plot $d_L(\sigma)$ for the critical value $\sigma_c = 0.97945$ determined previously. One expects then that the non-constant part comes entirely from the leading irrelevant operator. A fit to the form (3.10), also shown in Fig. 7, gives excellent results if we remove the data with $L \leq 6$. We obtain an exponent $x = 0.43(3)$. Thus we predict the existence of an irrelevant operator of dimension $2.43(3)$. We observed previously that $\sigma_c(L)$ converges linearly (in $1/L$) towards $\sigma_c(L \rightarrow +\infty)$, see Fig. 5. A simple calculation starting from eq.(3.10) shows that the correction is of order $L^{-(1/\nu+x)}$ and the linear correction corresponds to $x \simeq 0.33$. This is rather close to the numerical result, the difference being easily explained by taking into account further irrelevant operators.

4 Free energy and central charge

In this section, we use the free energy to deduce the central charge. We obtain results for both the $\pm J$ and the Gaussian distribution of disorder and compare these results to check universality.

As a byproduct of the measurements of the domain-wall free energy presented in the previous section, one also obtains the free energy $f_L^{(p)}$. We will first discuss the $\pm J$ disorder case. Averaging has been performed over sufficiently many samples to obtain statistical errors of typically $\delta f_L^{(p)} < 4 \cdot 10^{-6}$. Note that due to the aforementioned round-off error of one bond, p has an error of about 10^{-7} on the strip sizes considered which is not substantially below $\delta f_L^{(p)}$.

The (effective) central charge c can be estimated⁴ from this data since it appears as the universal coefficient of the first finite-size correction [40]

$$f_L^{(p)} = f_\infty^{(p)} + \frac{c \pi}{6L^2} + \dots \quad (4.1)$$

Note that the leading term $f_\infty^{(p)}$ is not universal. The universal $1/L^2$ term originates from the energy-momentum tensor T which has scaling dimension 2. The next correction is expected to arise from T^2 and should therefore give rise to a term of the form L^{-4}

$$f_L^{(p)} = f_\infty^{(p)} + \frac{c \pi}{6L^2} + \frac{d}{L^4} + \dots \quad (4.2)$$

Estimates for c are obtained by fitting the free energy data in intervals $L_0 \leq L \leq L_{\max}$ to (4.1) or (4.2). We have considered only intervals with $L_0 \leq L_{\max} - 3$ (at least four-point

⁴For a non-unitary theory what we call ‘ c ’ is in fact $c_{\text{eff}} = c - 12 \delta_{\min}$ where c is the central term in the operator product expansion of T with itself, and δ_{\min} the smallest dimension contributing to the free energy. See section 5.1 for further details.

fits). For a given form of the fit and interval of lattice sizes, we have chosen c to lie in the center of the resulting fits and adjusted the error to include all fits. The estimates for c obtained in this manner are shown in Fig. 8. Fits to (4.1) for lattice sizes $5 \leq L \leq 9$ are denoted by diagonal crosses and those for $6 \leq L \leq 12$ by plusses. Fits to (4.2) were performed for $4 \leq L_0 \leq 6$ with L_{\max} kept fixed at the largest available system size. The corresponding estimates are denoted by boxes.

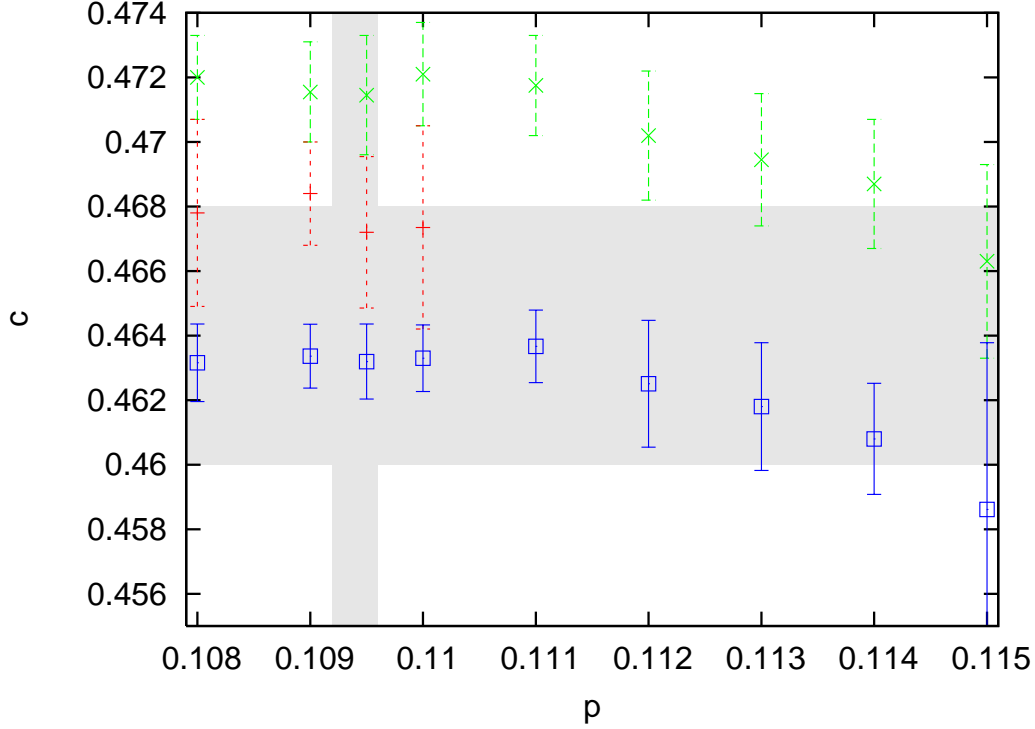


Figure 8: Estimates for the central charge c along the $\pm J$ Nishimori line (2.4) in the vicinity of the Nishimori point obtained from (4.1) for $5 \leq L \leq 9$ (' \times '), $6 \leq L \leq 12$ ('+') or (4.2) with $4 \leq L_0 \leq 6$ (boxes). The grey shaded areas denote our final confidence intervals for p_c (vertical) and the central charge (horizontal).

One notices that the estimates in Fig. 8 are almost independent of p in the range considered. On the one hand, this means that the estimates for c are stable. On the other hand, this implies that estimates for the central charge are not a good tool for locating the critical point precisely for the $\pm J$ distribution of disorder (the situation will be different for the Gaussian distribution, see below). Furthermore, one observes a slight trend of the fits (4.1) obtained with only a L^{-2} term to shift to smaller values as the range of system sizes considered is increased while the fits (4.2) with a L^{-4} term included converge rapidly with system size. Therefore, we quote as a final estimate with a generous error bar [15]

$$c = 0.464 \pm 0.004, \quad (4.3)$$

which is shown by the grey shaded horizontal bar (the estimate (3.4) for the location of the critical point p_c is shown by the grey shaded vertical bar). In any case, all estimates obtained from (4.1) with $L_{\max} = 12$ and $L_0 \geq 6$ satisfy $c < 0.469$. Furthermore, also

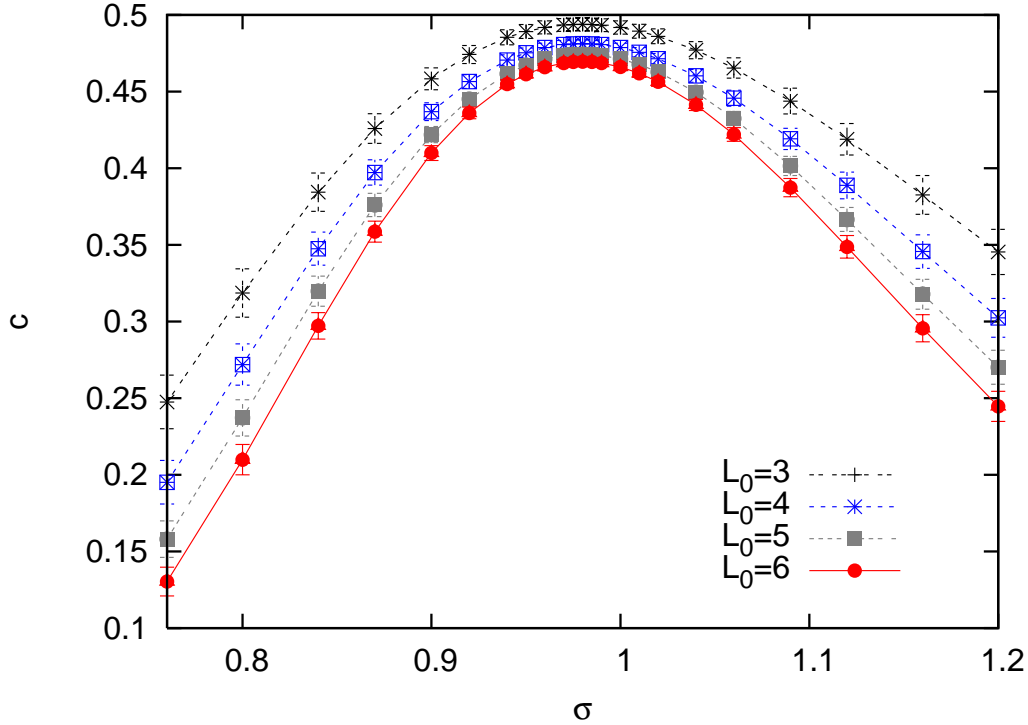


Figure 9: Central charge vs. σ along the Nishimori line for the Gaussian distribution of disorder, with $L_{\max} = 8$.

consideration of other possible finite-size corrections to (4.1) yields results which are consistent with (4.3). Thus, we can safely exclude the value $c = \frac{5\sqrt{3}\ln 2}{4\pi} \approx 0.47769$ for percolation in the Ising model [41] even if the absolute difference is not big.

We now turn to the Gaussian distribution of disorder. In this case, we will argue that the central charge, along the Nishimori line, gives a practical way of locating the multicritical point as the point where the estimates of the central charge have a maximum. We explained above that, for the $\pm J$ distribution, the estimate of the central charge was nearly independent of p making it difficult to locate the maximum. For the Gaussian distribution, the parameter p is replaced with the variance of the distribution σ , see eq. (2.5). Thus, the situation is different since it is possible to perform the simulations with the same disorder configuration for each variance σ . More precisely, one defines a bond J in the following way: $J = J_0 + \sigma j$, j being the random part obtained from a random number generator which we choose to be the same for different σ . As a consequence, most of the measurements will be correlated and in particular this will be true for the free energy and the deduced central charge (as was also the case for the domain-wall free energy measured in the previous section).

The central charge is shown in Fig. 9 where we present the effective central charge obtained by a fit to eq. (4.1) using free energies in the range $[L_0, L_{\max} = 8]$ for increasing L_0 . For the Gaussian distribution, we cannot suppress disorder fluctuations by fixing the number of bonds with a certain value globally. As a consequence, the data shown in Fig. 9 which has been extracted from runs of the same size as for the $\pm J$ disorder

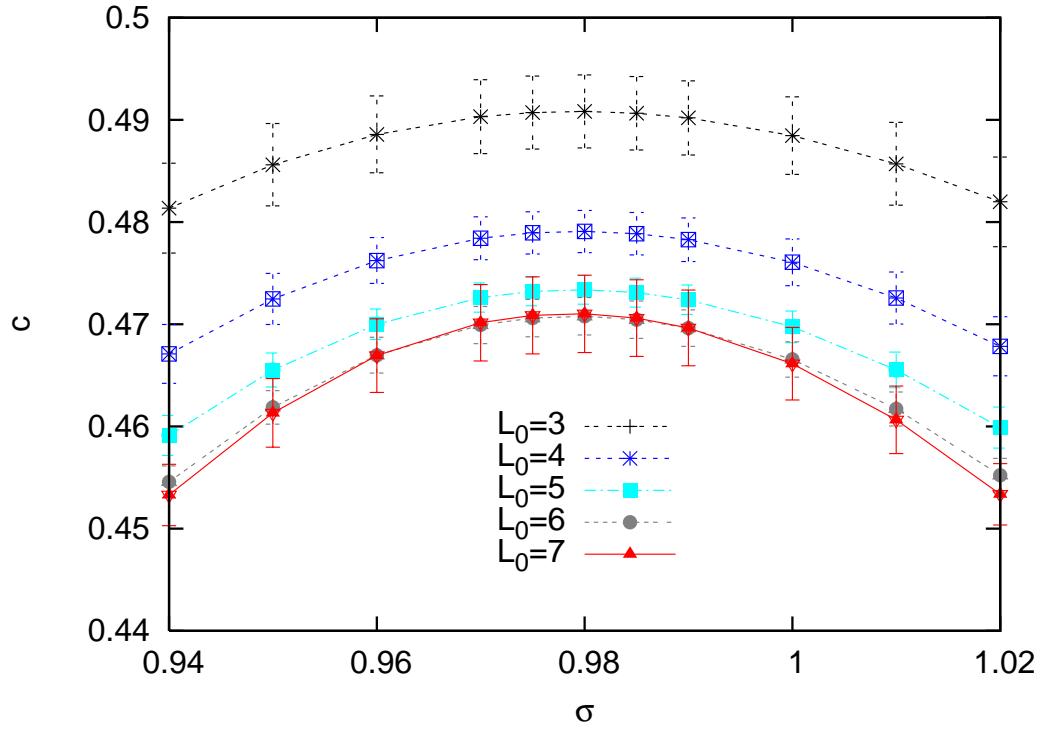


Figure 10: Central charge vs. σ along the Nishimori line for the Gaussian distribution of disorder close to the maximum $\sigma_c \simeq 0.98$ and with $L_{\max} = 10$.

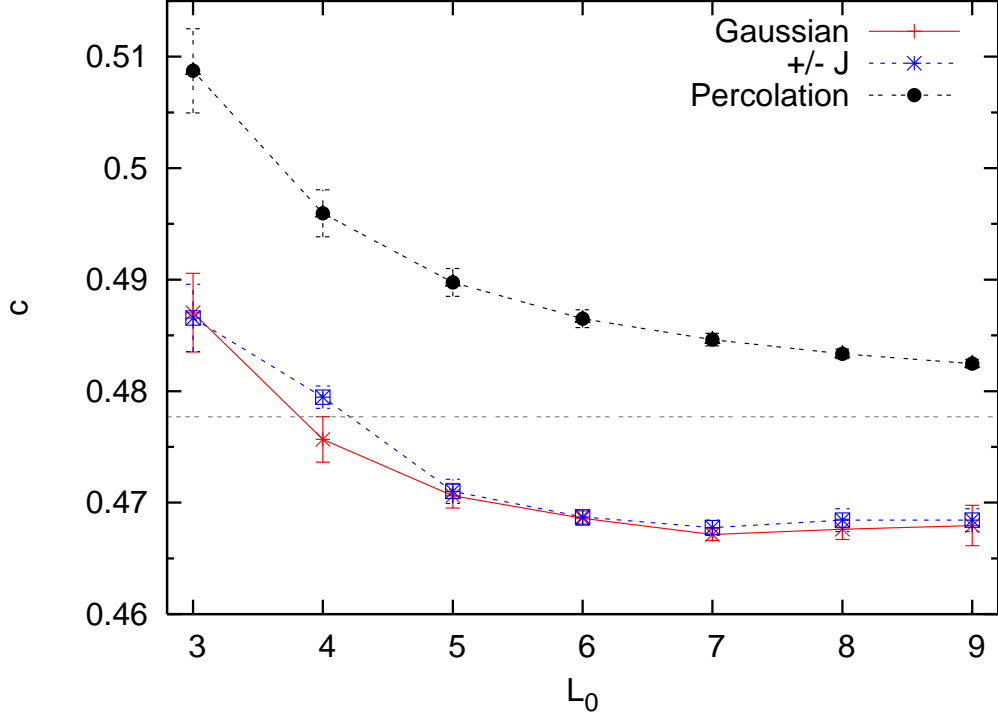


Figure 11: Central charge at the multicritical fixed point on the Nishimori line for the $\pm J$ and Gaussian distributions of disorder. We also show for comparison finite-size estimates of the central charge for percolation. The horizontal line shows the infinite system limit $c = \frac{5\sqrt{3}\ln 2}{4\pi}$ for percolation on Ising clusters [41].

(10 000 samples of strips of sizes $L \times 10^6$) has much bigger error bars. Still these larger error bars are partially compensated by the fact that the measurements are strongly sample-to-sample correlated, and thus the maximum is easy to identify: we have a stable maximum at $\sigma \simeq 0.98$. In Fig. 10, we show the measured central charge close to the maximum with $L_{\max} = 10$. An estimate of the maximum gives for all the ranges of L employed a value of $\sigma_c \simeq 0.9805 \pm 0.0005$, with no measurable change of the central charge compared to $\sigma = 0.98$. For the size that we consider here, the agreement is very good with the $\sigma_c(L)$ obtained with the domain-wall measurements, see Fig. 5. Additional runs were performed for the value $\sigma = 0.98$, in particular for larger sizes, up to $L = 12$. For $\sigma = 0.98$ the average is performed over at least 20 000 samples, each sample being a strip of size $L \times 10^7$. We will employ in the following this data to compute the central charge that we will compare to the $\pm J$ disorder case. In Fig. 11, we compare the effective central charges obtained for the Gaussian and the $\pm J$ distributions of disorder. For the $\pm J$ distribution, we employed the data for $p = 0.1095$. For comparison, we also show the central charge obtained for percolation on an Ising model. In all these cases, we show the central charge obtained by a fit to (4.1) for increasing L_0 while keeping the maximum size fixed to $L_{\max} = 12$. The agreement between the two types of disorder is excellent. We see that the central charges converge to $\simeq 0.465$ at the multicritical fixed point on the Nishimori line for both cases of disorder. We thus have strong evidence of

the universality of the multicritical fixed point. Moreover, the asymptotic value is clearly different from the value of percolation, either the numerical one on a finite system or the infinite system limit also shown in Fig. 11.

5 Spin-spin correlation functions

In the previous sections, we have already seen that the universality class of the multicritical point on the Nishimori line, for the two types of disorder considered, is different from the one of percolation. Still the central charge is very close and it is then useful to find further measurements to confirm this result. In this section, we present numerical results for the spin-spin correlation functions on the Nishimori line close to the Nishimori point.

A general correlation function C_n between two points \vec{r}_1 and \vec{r}_2 has the following power-law form with exponent $2x_n$ in a two-dimensional conformal field theory on the infinite plane:

$$C_n(\vec{r}_1, \vec{r}_2) \propto \frac{1}{|\vec{r}_1 - \vec{r}_2|^{2x_n}}. \quad (5.1)$$

In the transfer matrix computations we use long strips with periodic boundary conditions along the short directions which one can also interpret as a cylinder. Therefore, we consider the correlation function C_n on the infinite cylinder of circumference L with coordinates $u \in [1, L]$ and $v \in]-\infty, +\infty[$. Applying a conformal mapping to (5.1), one infers the following behaviour on the cylinder (see, e.g., chapter 11.2 of [42])

$$C_n((u_1, v_1), (u_2, v_2)) \propto \frac{(\frac{2\pi}{L})^{2x_n}}{\{2 \cosh(2\pi(v_1 - v_2)/L) - 2 \cos(2\pi(u_1 - u_2)/L)\}^{x_n}}. \quad (5.2)$$

There are two particular cases that we will consider in the following:

- $v_1 = v_2$, $u = u_1 - u_2$. The correlation function is measured for two points across the strip, separated by a distance u . The correlation function takes the form:

$$C_n(0, u) \propto \left(\sin\left(\frac{\pi u}{L}\right) L \right)^{-2x_n}. \quad (5.3)$$

One can then extract the exponent $2x_n$ by a direct fit of the measured correlation function, after averaging over the disorder, to this form. One disadvantage of this method is that we can use only points separated by distances $u \leq L/2$.

- When one chooses $u_1 = u_2$, $v = v_1 - v_2$ the correlation function takes the following form:

$$C_n(0, v) \propto \left(\sinh\left(\frac{\pi v}{L}\right) L \right)^{-2x_n}. \quad (5.4)$$

Thus we consider two points separated along the strip with the same position across the strip, and it is possible to access long distances.

We will apply these two forms to the n th moments of the spin-spin correlation function $[\langle S(u_1, v_1)S(u_2, v_2) \rangle^n]$, where $[\cdots]$ stands for the average over disorder. The general result is then, for the two cases discussed above:

$$\begin{aligned} [\langle S(0)S(x) \rangle^n] &\propto \left(\sin\left(\frac{\pi x}{L}\right)L \right)^{-\eta_n}, \\ [\langle S(0)S(y) \rangle^n] &\propto \left(\sinh\left(\frac{\pi y}{L}\right)L \right)^{-\eta_n}. \end{aligned} \quad (5.5)$$

Here, we have identified $\eta_n = 2x_n$. All along the Nishimori line, the moments of these correlation functions are equal two by two [2], thus we have the general result that $\eta_{2k-1} = \eta_{2k}$. For a pure system, one has $\eta_n = n \times \eta$. On the other hand, in the case of percolation over Ising clusters, it is easy to see that all moments of the spin-spin correlation functions are equal (and not only two by two). Then, if the Nishimori point would be in the percolation universality class, the exponents for the correlation functions should collapse to a unique value $\eta_n = \eta$ at the critical point.

As a first measurement for $\pm J$ disorder, we show in Fig. 12 the effective magnetic exponent η_1 that we obtain from a fit to the form eq. (5.3). The effective magnetic exponent η_1 was computed for three points on the Nishimori line: at $p = 0.105$, which is well inside the ferromagnetic phase and indeed, we see that the effective magnetic exponent tends to a small value; at $p = 0.115$ which is well in the paramagnetic phase, which is confirmed by the fact that the effective magnetic exponent increases; at $p = 0.1095 \simeq p_c$ where the effective magnetic exponent seems to converge to a value $\eta_1 \simeq 0.185$. On this figure, we also show the corresponding magnetic exponent obtained from simulations of the pure Ising model and also of the percolation model, as well as the expected values for these two models in the infinite limit ($\eta = \frac{1}{4}$ and $\frac{5}{24}$, respectively – see, e.g., [43] and [37], respectively). These two measurements are presented in order to show what type of correction we can expect in such a measurement of the magnetic exponent. Indeed, we can see that this method gives rather accurate measurements for large L (for $L = 12$, the deviation is around 1%). From this, we can conclude that the value of η_1 for $p = 0.1095$ is significantly distinct from the one of percolation. This is an additional proof that the multicritical point on the Nishimori line is not in the universality class of percolation.

Next, in Fig. 13, we show the same quantity but only close to the critical point. In this figure, one can clearly distinguish a change of behaviour close to $p \simeq 0.1095$. For lower p , the exponent decreases, which is expected since we are in the ferromagnetic phase. On the contrary, for p larger than 0.1095, we observe that the magnetic exponent increases, as expected since we are in the paramagnetic phase.

Fig. 14 shows the moments of the spin-spin correlation function for $L = 20$ and $p = 0.1095$. There is a similar plot in [15], but the present data set is completely independent. The present data was obtained for a geometry which differs from [15], namely on 4001×20 strips with a globally fixed number of positive (negative) bonds while for that of [15], each bond was assigned a value independently. Here we have discarded the 1000 initial (and final) iterations before taking 101 measurements of the correlation functions every 20 iterations. The data in Fig. 14 was obtained by averaging over 7623 such strips, resulting in statistical error bars which are much smaller than the size of the symbols. Despite these differences, the present results for $[\langle S(0)S(x) \rangle^n]$ agree with those of [15] within error bars.

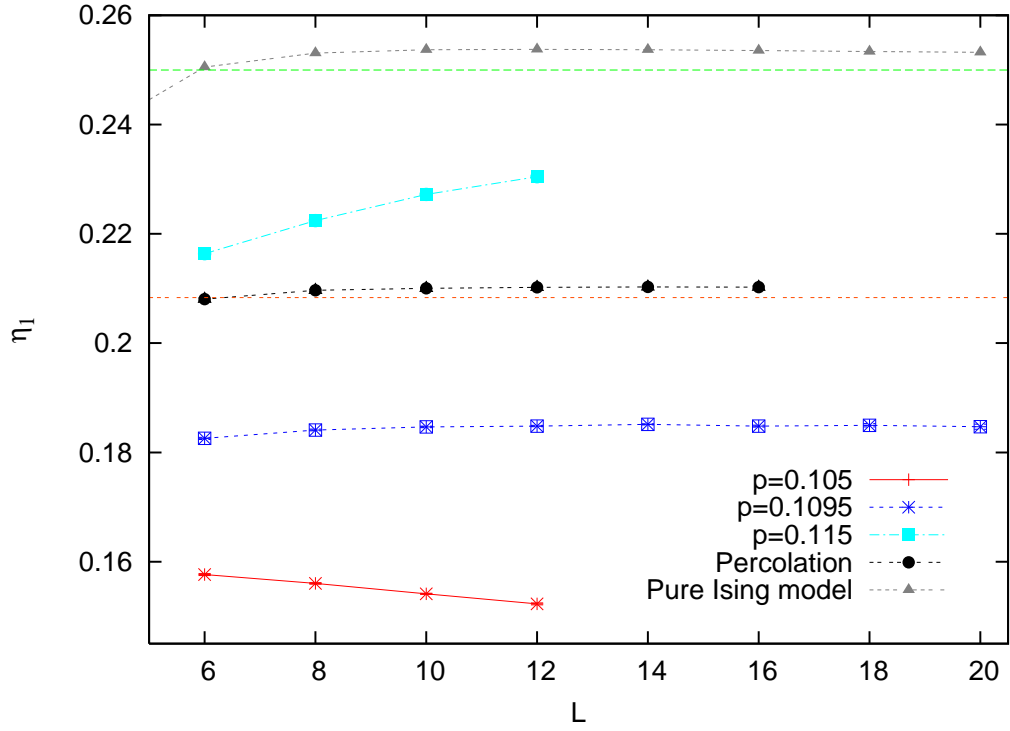


Figure 12: Effective magnetic exponent η_1 for the $\pm J$ RBIM with $p = 0.105$, $p = 0.1095$, $p = 0.115$, the percolation model and the pure Ising model.

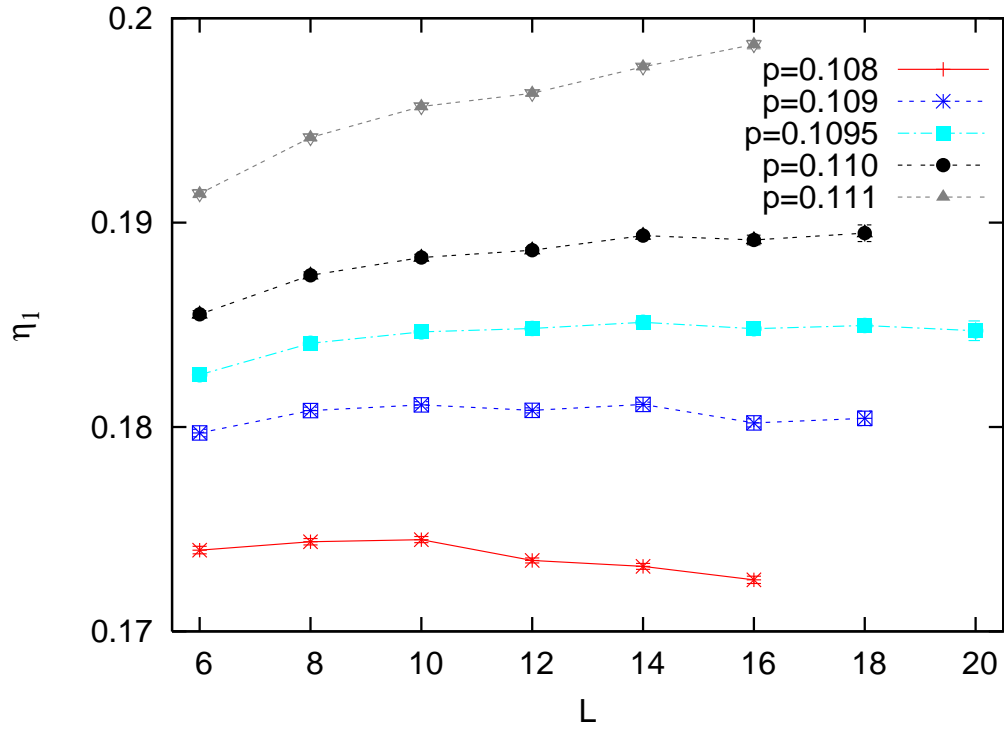


Figure 13: Effective magnetic exponent η_1 for $p = 0.108, \dots, 0.111$, for the $\pm J$ disorder on the Nishimori line.

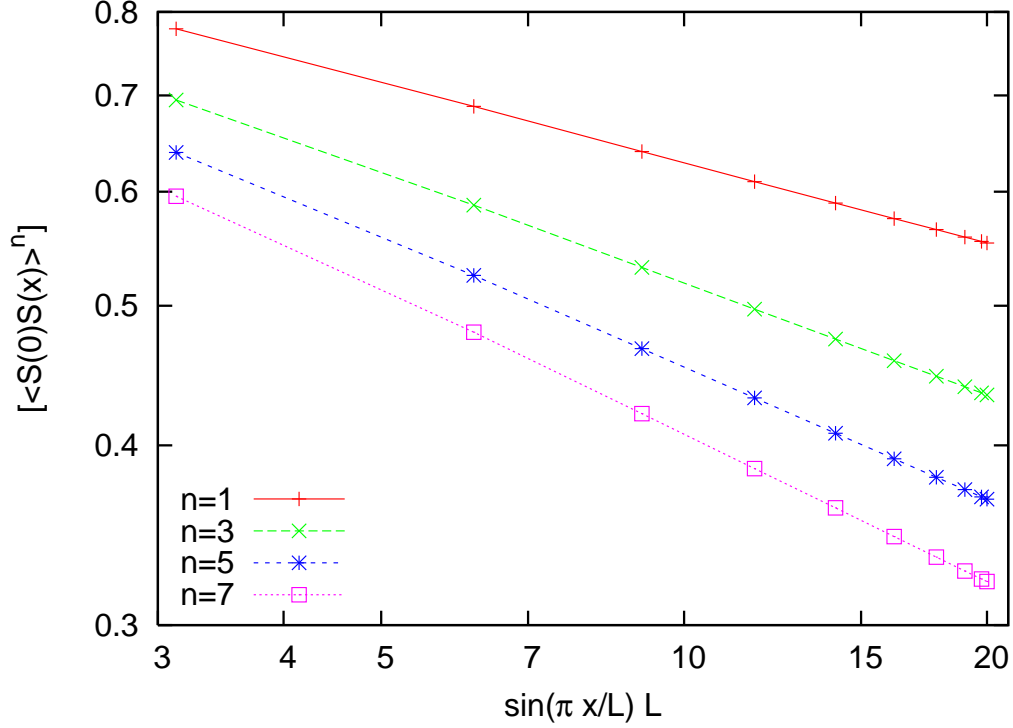


Figure 14: Moments of the spin-spin correlation function for the $\pm J$ RBIM with $p = 0.1095$ and $L = 20$. We only show the odd moments. Error bars are much smaller than the size of the symbols.

A direct fit on a doubly logarithmic scale of the correlation functions for $p_c = 0.1095$ and $L = 20$ to the form (5.3) yields:

$$\begin{aligned}
 \eta_1 &= \eta_2 = 0.1848 \pm 0.0003, \\
 \eta_3 &= \eta_4 = 0.2552 \pm 0.0009, \\
 \eta_5 &= \eta_6 = 0.3004 \pm 0.0013, \\
 \eta_7 &= \eta_8 = 0.3341 \pm 0.0016.
 \end{aligned} \tag{5.6}$$

These estimates are consistent with those of [15, 44] within error bars.

We now turn to the Gaussian distribution of disorder. In Fig. 15, we present the exponent η_1 obtained from a direct fit with eq. (5.3) in function of σ . For that case, we have data for size up to $L = 14$ and for each value of L and σ we average over 10 000 samples of geometry $L \times 200 L$. We clearly see a crossing of the curves close to $\sigma = 0.98$, in agreement with the previous results. At the crossing point, we have $\eta_1 \simeq 0.18$, which is very close to the corresponding value for the $\pm J$ distribution of disorder.

Next, we present the exponents obtained, again for $L = 14$, from a direct fit on a doubly logarithmic scale to the correlation functions for $\sigma = 0.98$:

$$\eta_1 = \eta_2 = 0.1818 \pm 0.0002,$$

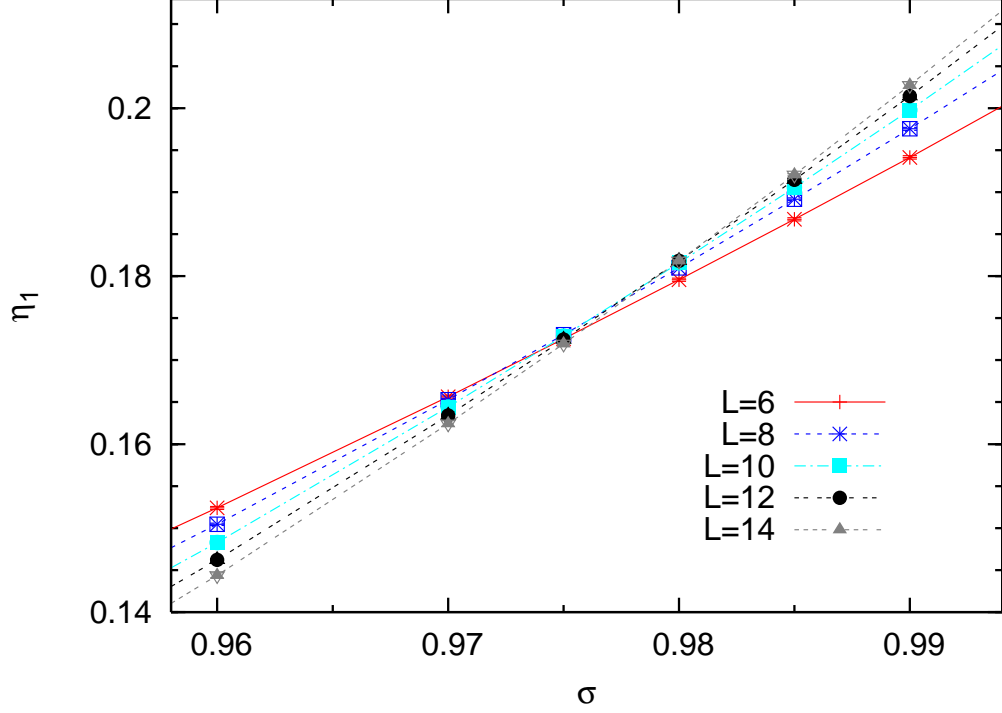


Figure 15: Effective magnetic exponent η_1 vs. L for the Gaussian distribution of disorder.

$$\begin{aligned}
 \eta_3 &= \eta_4 = 0.2559 \pm 0.0002, \\
 \eta_5 &= \eta_6 = 0.3041 \pm 0.0002, \\
 \eta_7 &= \eta_8 = 0.3402 \pm 0.0002.
 \end{aligned} \tag{5.7}$$

The value of these exponents is close to the ones for the $\pm J$ distribution of disorder. Note that there is still a small difference, $\eta_1^{\pm J} \simeq 0.1848$ compared to $\eta_1^{\text{Gaussian}} \simeq 0.1818$. This difference is due to the fact that the exponents are obtained only close to the critical points. For the $\pm J$ disorder case, the measurement is done at $p = 0.1095$. From Fig. 13, one can read off that this will imply a change of order 0.002 on η_1 if we take $p_c = 0.1093$. Taking into account this correction, the correspondence of η_1 is nearly perfect between the two types of disorder, thus giving more support for the universality.

In Fig. 16, we show the exponent η_1 obtained by an independent set of simulations on a geometry $L \times 100L$ and with the measurement of the correlation function *along* the strip. We simulated 10 000 samples for each size up to $L = 12$ with this geometry. The exponent η_1 is obtained from a fit with eq. (5.4). To perform the fit, we keep only the data for correlation functions with two points at a distance y such that $10 \leq y \leq 10 \times L$. Thus one does not use the data for two operators very close, contrary to what is done while fitting with eq. (5.3) and we expect to reduce the finite-size corrections. In Fig. 16, one sees that for the largest L , one obtains a constant exponent for $\sigma = 0.98 - 0.981$ with $\eta_1 = 0.180 - 0.182$. Thus these results are in perfect agreement with the previous measurements on a different geometry.

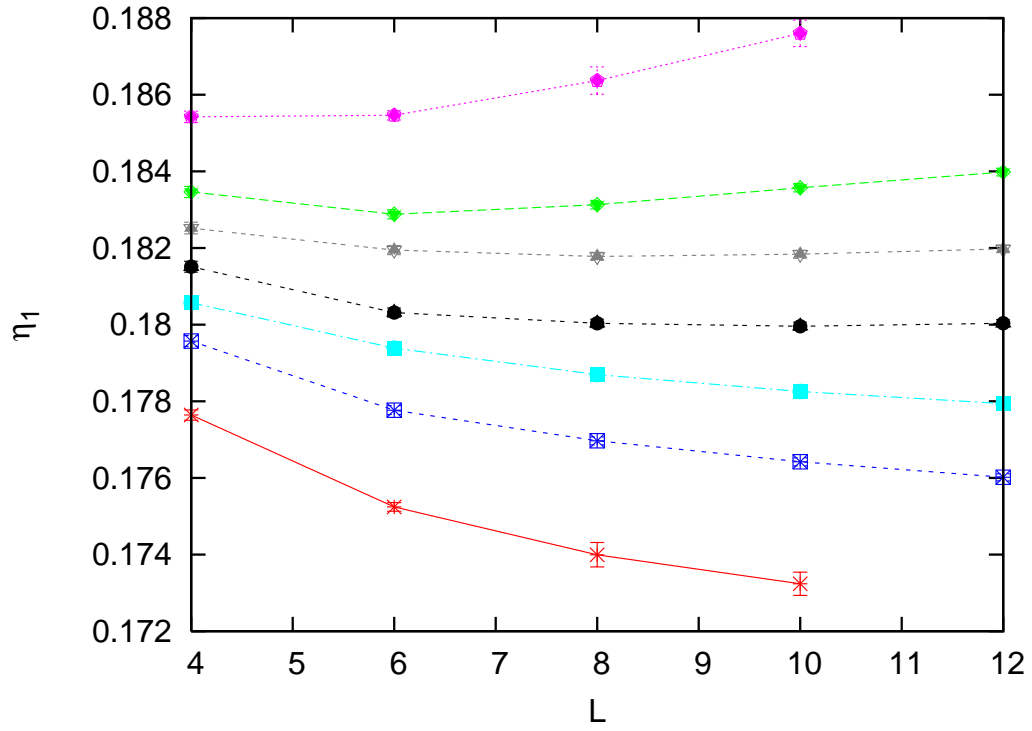


Figure 16: Effective magnetic exponent η_1 vs. L for the Gaussian distribution of disorder with $\sigma = 0.976, 0.978, 0.979, 0.980, 0.981, 0.982, 0.984$ (from bottom to top).

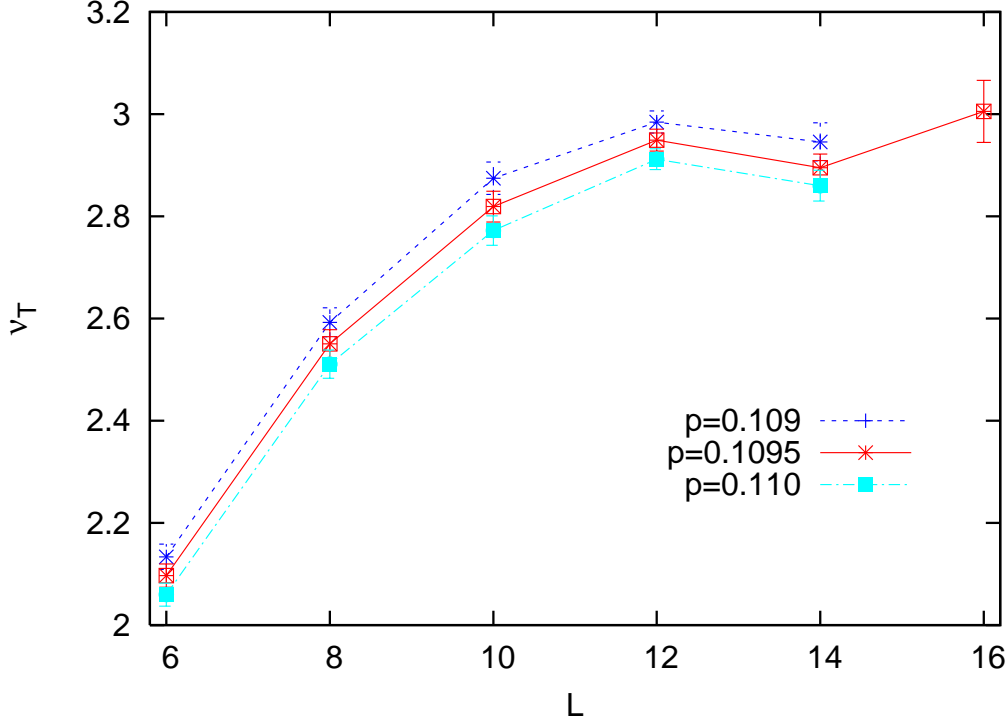


Figure 17: Thermal exponent ν_T vs. L for the $\pm J$ distribution of disorder.

Finally, in Fig. 17, we present results for the correlation function of the energy operator $\epsilon_{ij} = J_{ij} S_i S_j$. A thermal exponent ν_T is associated to this operator, which corresponds to a perturbation in temperature, via the relation

$$\nu_T = \frac{1}{(2 - x_T)} . \quad (5.8)$$

This exponent replaces the exponent x_n in eq. (5.3) if we replace the spin operator with the energy operator. In Fig. 17, ν_T is shown for $p \simeq p_c$ and for increasing strip widths L . Finite-size corrections are very strong for ν_T . We obtain a value of $\nu_T \simeq 3$ for $L = 14, \dots, 16$, but it is not clear if we have reached a large enough size. With a different method, Merz and Chalker [19] obtained a value of $\nu_T = 4 \pm 0.5$ by measurements on system sizes up to $L = 32$. We believe that the extrapolation of our results for larger sizes is compatible with this result.

5.1 Central charge and magnetic exponents

We now return to the central charge. We mentioned at the beginning of section 4 that the measured central charge is an effective quantity which can be affected by operators with negative dimensions. Indeed, if one considers a torus, *i.e.* a strip of geometry $M \times L$ with periodic boundary conditions in both directions, one has the relation [45]

$$\frac{Z}{Z_{\text{bulk}}} = Q^{-c/12} \sum_{a,b} N_{a,b} Q^{\delta_a + n_b} \quad (5.9)$$

with

$$Q = e^{-2\pi \frac{M}{L}}. \quad (5.10)$$

Here, the index a is associated to the primary operators ϕ_a which appear in the transfer matrix, while the index n_b is non zero (and positive) for the conformal descendants only. $N_{a,b}$ counts the multiplicity of the descendants of the operator ϕ_a at the level b . Next, we consider the free energy per spin:

$$f(L, M) = \frac{\ln Z(M, L)}{ML} = f_{\text{bulk}} + \frac{c\pi}{6L^2} + \frac{1}{ML} \ln \left[\sum_{a,b} N_{a,b} Q^{\delta_a + n_b} \right]. \quad (5.11)$$

If all the operators which appear in the transfer matrix have a non-negative dimension, then in the limit $M \gg L$, the last term in eq. (5.11) can be dropped and one recovers eq. (4.1). On the contrary, if an operator with a negative dimension is present in the transfer matrix, then for large M , the last term in eq. (5.11) will be dominated by this operator. Let us call $\delta < 0$ the dimension associated to the operator with the lowest dimension. Then eq. (5.11) will become, in the limit $M \gg L$:

$$f(L, M) = f_{\text{bulk}} + \frac{\pi}{6L^2}(c - 12\delta) + \dots \quad (5.12)$$

Thus, if a negative dimension operator appears in the transfer matrix, the measured central charge will be only an effective quantity $c_{\text{eff}} = c - 12\delta > c$. If no negative dimension operators appear in the transfer matrix, then one has $\delta = 0$ since the identity operator with zero dimension is always present.

It is known that negative exponents arise at the Nishimori point in certain moments of the correlation functions of the disorder operator [20]. Still, these operators will not cause any problems in the present context since the disorder operator is not a local operator of our theory.

We know of no direct way to determine if an operator with a negative dimension is present in the transfer matrix. Still, one can make the following simple test. In the pure Ising model, the lowest dimension corresponds to the magnetic operator. Since one expects that the magnetic exponent is present and we know that its dimension is small, one can compare it with the first dimension which appears in eq. (5.11). Assuming that there is no negative dimension operator in the transfer matrix, the last part of eq. (5.11) takes the form

$$\frac{1}{ML} \ln \left(1 + e^{(-2\pi \frac{M}{L} \delta_1)} + \dots \right) \quad (5.13)$$

with δ_1 the lowest dimension. Thus, by computing

$$\ln \left(e^{ML(f(L,M) - f(L, M \rightarrow +\infty))} - 1 \right) \simeq -2\pi \frac{M}{L} \delta_1 + \dots, \quad (5.14)$$

one can estimate directly δ_1 . In Fig. 18, we show this quantity for $L = 4, 6$ and 8 , as well as a fit to the data in the range $1.5 \leq M/L \leq 5$. These bounds are selected by imposing a good quality of the fit. The values extracted for δ_1 are $0.108(1), 0.104(1), 0.102(1)$ for $L = 4, 6, 8$, respectively. These values seem to converge to a value close to the one of the magnetic exponent $\eta_1/2 \simeq 0.0925$ such that it is reasonable to identify it with the magnetic operator. This suggests that the measured central charge is indeed the real central charge.

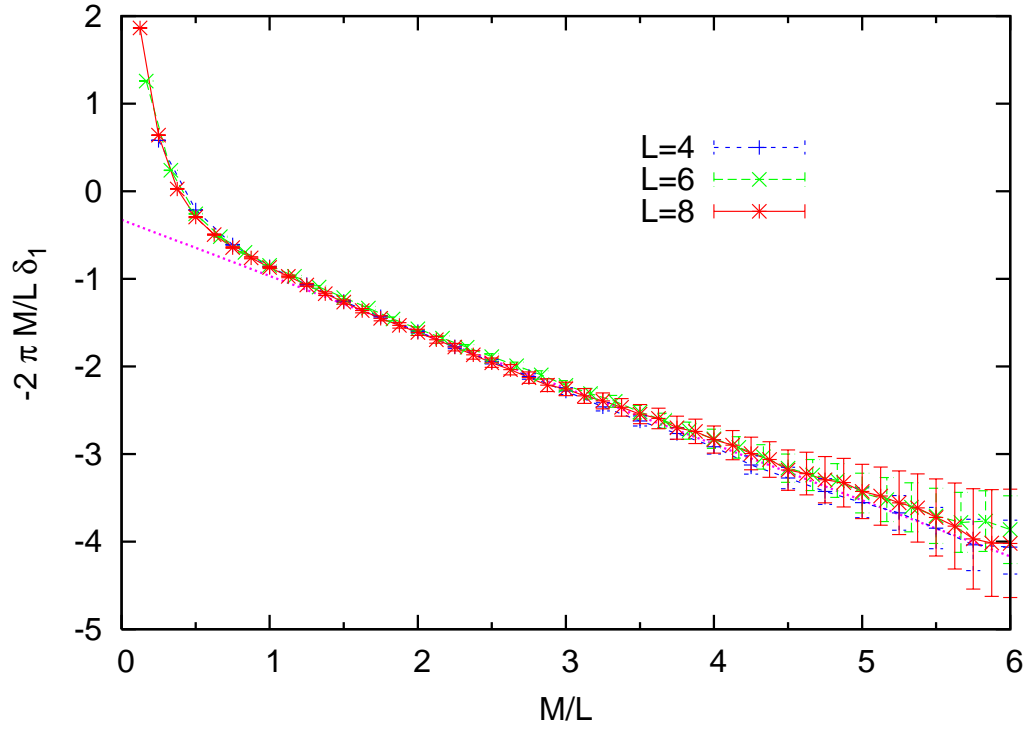


Figure 18: Fit of the free energy for the $\pm J$ RBIM with $p = 0.1094$ to the form (5.14) in the range $1.5 \leq M/L \leq 5$ for $L = 4, 6$ and 8 .

6 Other measurements

In this section, we present measurements of other quantities, namely the Binder cumulant and the magnetic susceptibility. For each of these quantities, we do not expect to improve precision, the measurements are rather done in order to check the consistency of the previous measurements.

6.1 Binder cumulant

We first present measurements of the magnetic Binder cumulant on the Nishimori line, in order to perform an independent measurement of the critical p for the $\pm J$ RBIM. The magnetic Binder cumulant is defined as follows in terms of the moments of the magnetization m [46, 47]:

$$B(L) = \frac{1}{2} \left(3 - \frac{[\langle m^4 \rangle]}{[\langle m^2 \rangle]^2} \right). \quad (6.1)$$

We note that on the Nishimori line the magnetic Binder cumulant is identical with the overlap Binder cumulant which is usually employed in measurements for spin-glass models, since we have an equality of the first and second moment of the spin-spin correlation functions [2].

Simulations are performed on square lattices with periodic boundary conditions in both directions and with linear sizes in the range $L = 3$ up to $L = 8$. We employ the transfer matrix to compute the partition function without and with a small magnetic field h as well as with $2h$. Then we extract the second and fourth moment of the magnetization m from the expansion

$$Z(h) = Z(h=0) \left(1 + \frac{h^2}{2} \langle m^2 \rangle + \frac{h^4}{4!} \langle m^4 \rangle + \dots \right), \quad (6.2)$$

and a similar expansion of $Z(2h)$. The terms $\langle m \rangle$ and $\langle m^3 \rangle$ do not appear in the expansion since they vanish at $h = 0$ on a finite system. We used a value of $h \simeq 0.01/L^2$ in our simulations. In order to reach a good precision, a large number of samples had to be simulated, typically one million samples for each size and value of disorder p . Fig. 19 shows a plot of the Binder cumulant versus p . In this figure, we observe a crossing in the expected region, *i.e.* $p \simeq 0.11$. Since the number of samples that we have to simulate is huge, it is difficult to reach sizes large enough to improve the previous estimate of the critical point on the Nishimori line. Thus the measurements that we show here should be regarded as a consistency test only.

The inset of Fig. 19 shows a plot of the Binder cumulant versus the rescaled variable, $(p-p_c) L^{1/\nu}$. Assuming the values that we obtained in section 3, $p_c = 0.1094$ and $\nu = 3/2$, we see that we have a good scaling behaviour of the Binder cumulant already for small lattices.

6.2 Susceptibility

A second quantity of interest is the susceptibility χ , which we measure using the transfer matrix. We compute the free energy, first without any applied magnetic, and next with

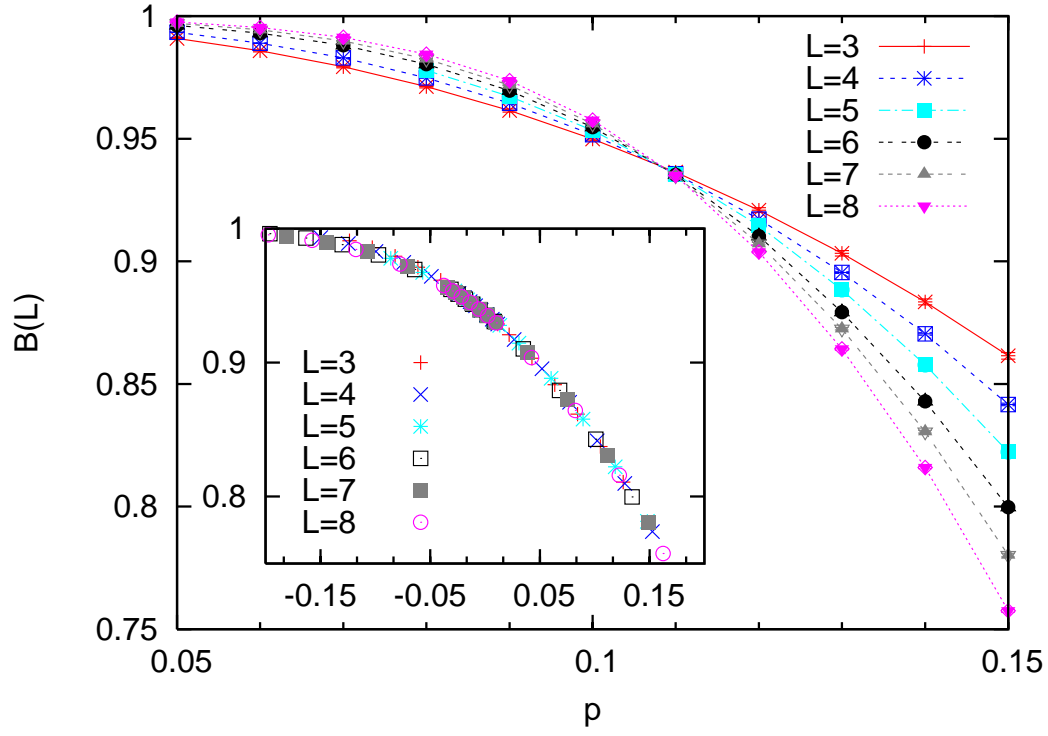


Figure 19: $B(L)$ vs. p on the Nishimori line for the $\pm J$ disorder case. The inset shows $B(L)$ vs. $(p - p_c)L^{1/\nu}$, with $p_c = 0.1094$ and $\nu = 3/2$.

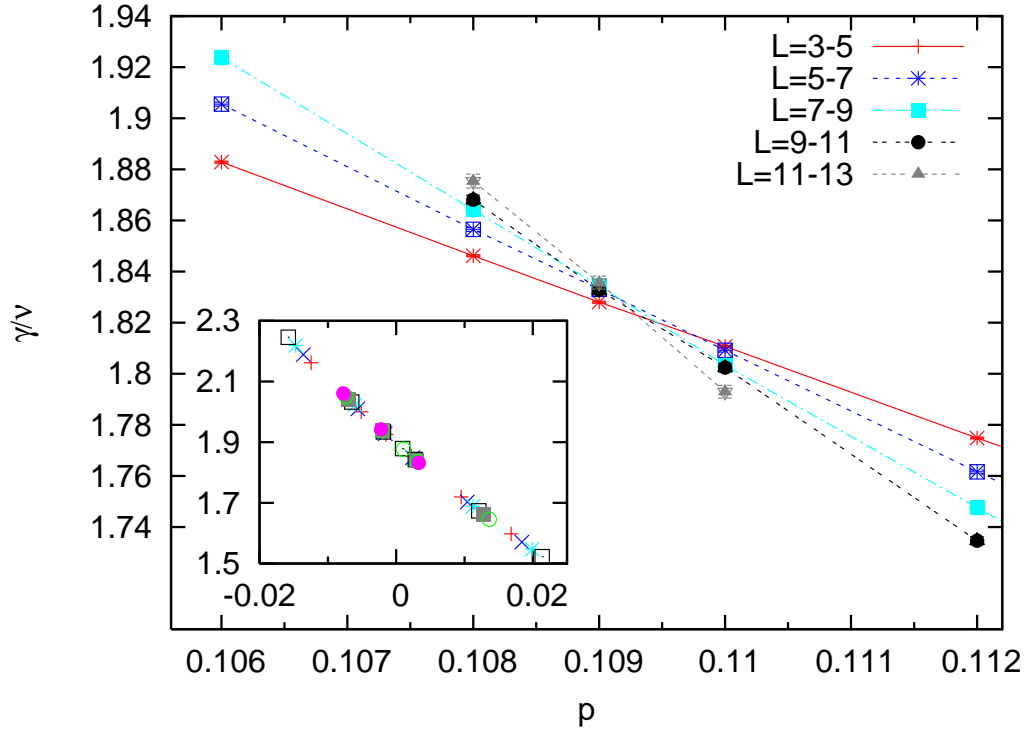


Figure 20: Susceptibility exponent γ/ν vs. p on the Nishimori line for the $\pm J$ disorder case. The inset shows $\chi(L)L^{-\gamma/\nu}$ vs. $(p - p_c)L^{1/\nu}$, with $p_c = 0.1094$ and $\nu = 3/2$.

a small magnetic field. $f_L(0)$ and $f_L(h)$ are determined with the same realization of disorder in order to decrease the fluctuations. The susceptibility is obtained by the following relation

$$f_L(h) - f_L(0) \simeq (\beta h)^2 \chi(L) . \quad (6.3)$$

We need to choose a very small magnetic field h , typically $h \simeq 0.000001$, in order to ensure that we do not have a magnetic term.

We expect that the susceptibility is of the form $\chi(L) \simeq L^{\gamma/\nu}$ at a critical point. In Fig. 20, we present the effective susceptibility exponent obtained by two-point fits for data with odd sizes. For each of these points, we made 10 000 measurements on strips of sizes $L \times 10^5$. We see that the crossing converges towards a value of p close to 0.109. Moreover, we can see that the value of the susceptibility exponent seems to converge to a value close to $\gamma/\nu \simeq 1.82$. Thus one can also check that the hyperscaling relation $\gamma/\nu + 2\beta/\nu = d$ is satisfied with $2\beta/\nu = \eta_1 \simeq 0.18$.

Finally, we can also use the measured values of the susceptibility to perform a fit in the following form

$$\chi(L) \simeq L^{\gamma/\nu} a((p - p_c)L^{1/\nu}) . \quad (6.4)$$

Since this fit involves three parameters, we obtain a large error bar on each of them. Keeping only the reasonable fits, one obtains good collapses of the data in the following range: $\gamma/\nu = 1.8 - 1.82$, $p_c = 0.109 - 0.110$, $1/\nu = 0.65 - 0.7$. In the inset of Fig. 20 we present a plot of $\chi(L)L^{-\gamma/\nu}$ vs. the rescaled variable $(p - p_c)L^{1/\nu}$ with the values $p_c = 0.1094$, $1/\nu = 2/3$ and $\gamma/\nu = 1.82$ with an excellent collapse of the data.

7 Dilution

In this section, we will consider the more general case of a binary distribution with dilution. We denote by q the amount of dilution and by p the amount of disorder (see section 2 for the definitions). The Nishimori line is now replaced by a surface in the $T - p - q$ space. For $p = 0$, we expect only two critical points [36]: an attractive point for $q = 0$ (no dilution) and a repulsive point for $q = 0.5$ which is a percolation fixed point (see figure 2) and is on the Nishimori surface. Another fixed point, also on the Nishimori surface, is the fixed point on the Nishimori line determined previously for $q = 0$. In this section we want to study the flow between these two fixed points on the Nishimori surface. In particular, obtaining a clear flow between these two fixed points will give further evidence that the multicritical point on the Nishimori line (*i.e.* without dilution) is not in the same universality class as percolation. Our measurements are carried out as follows: for a fixed dilution q , we perform simulations for varying p and T in the Nishimori surface defined in eq. (2.8) and look for a maximum in the effective central charge. Next we check the value of this maximum $c_{\text{eff}}(q)$ vs. q which is shown in Fig. 21, for central charges obtained numerically with a fit to the form eq. (4.1) for the sizes $[4, 5, 6, 7, 8]$, $[5, 6, 7, 8]$ and $[6, 7, 8]$. As expected, $c_{\text{eff}}(q)$ varies monotonically between $c_{\text{eff}}(q = 0)$ and $c_{\text{eff}}(q = 0.5)$ showing that there is no additional fixed point.

In practice, since c_{eff} changes on a very small range (between 0.47769 for $q = 0.5$ and $\simeq 0.464$ for $q = 0$) with strong finite-size corrections, it is more convenient to consider

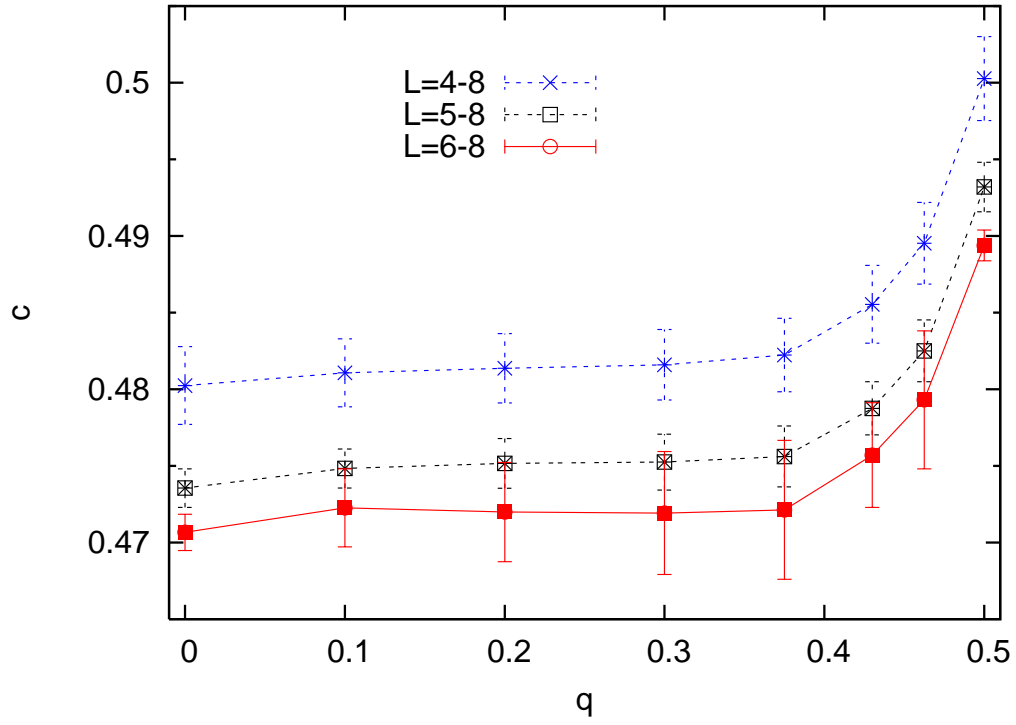


Figure 21: Central charge vs. dilution q along the intersection of the $p-q-T$ Nishimori surface with the paramagnetic-ferromagnetic critical surface for the $\pm J$ disorder case.

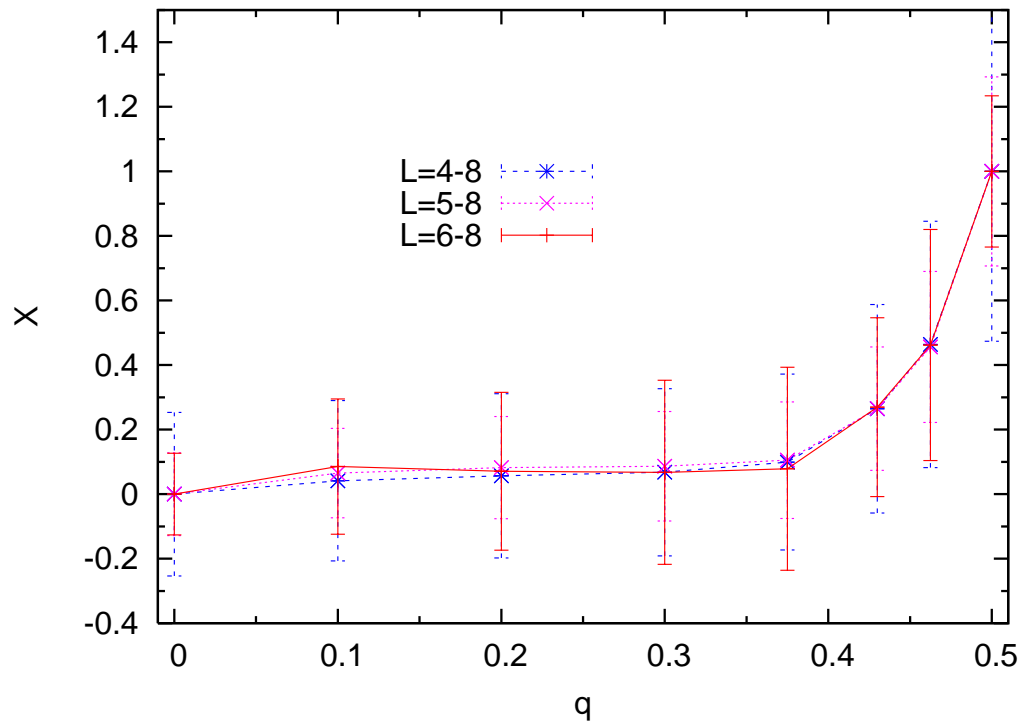


Figure 22: X vs. dilution q along the intersection of the $p - q - T$ Nishimori surface with the paramagnetic-ferromagnetic critical surface for the $\pm J$ disorder case.

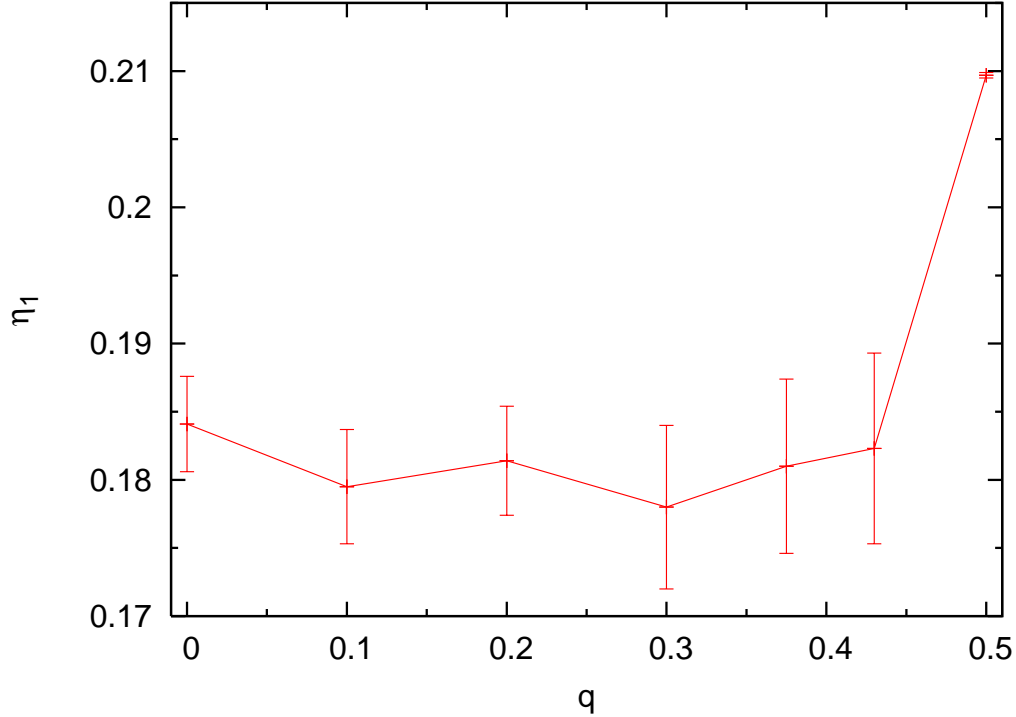


Figure 23: Magnetic exponent η vs. dilution q along the intersection of the $p - q - T$ Nishimori surface with the paramagnetic-ferromagnetic critical surface for the $\pm J$ disorder case.

the following quantity:

$$X = \frac{c_{\text{eff}} - c_{\text{eff}}(0)}{c_{\text{eff}}(0.5) - c_{\text{eff}}(0)}, \quad (7.1)$$

where for each range of sizes L we consider the values obtained with the same corrections for $c_{\text{eff}}(0)$ and $c_{\text{eff}}(0.5)$. By construction, this quantity is equal to zero at $q = 0$ (no dilution) and is equal to 1 at $q = 0.5$ (the percolation case). Fig. 22 shows the quantity X as a function of dilution q , again for the sizes $[4, 5, 6, 7, 8]$, $[5, 6, 7, 8]$ and $[6, 7, 8]$. Apart from the size of the errors, one does not observe significant differences. In all cases, one immediately sees that the central charge is dominated by the behaviour of the fixed point without dilution. If one starts at the percolation point, a small decrease in q will appear as a jump towards the fixed point without dilution ($q = 0$)⁵. At $q \simeq 0.4$, X is already indistinguishable from zero, indicating that the central charge is the same as the one for $q = 0$. One expects that by increasing the sizes of the data in the fit for determining c_{eff} , one should observe a crossover between the two fixed points $q = 0.5$ and $q = 0$ (such an effect will be shown in the next section for the flow between the Nishimori point and the fixed point of the pure Ising model). Here we cannot really observe this effect since the crossover is too fast.

⁵More precisely, critical properties at finite temperature are expected to be controlled by the fixed point N' in Fig. 2 [4]. Fortunately, the crossover scale for the flow between N and N' appears to be so small that this difference can be neglected in practice.

Finally, Fig. 23 shows the magnetic exponent vs. the dilution measured on long strips of width $L = 8$. Here again, we observe the same effect. For $q = 0.5$, the magnetic exponent is known exactly, it is $\eta = 5/24 \simeq 0.208333$ [37]. As we decrease q , the magnetic exponent jumps to a value compatible with the one of the multicritical point on the Nishimori line $\eta \simeq 0.18$.

8 Out of the Nishimori line

In this section, we present some results off the Nishimori line. We will consider two cases separately. First we investigate the line which corresponds to the flow from the Nishimori point to the pure Ising model. This line corresponds to the ferromagnetic-paramagnetic transition line. We show in the next subsection that this line can be determined from the maximum of the central charge when varying temperature at fixed p . We show further that the flow on this line is from the Nishimori point towards the pure Ising model fixed point. Next we turn to the line which connects the Nishimori point with a fixed point at zero temperature. An important issue concerns the verticality or re-entrance of this line. By arguing that the nature of the Ferro-Para transition at the Nishimori point is of geometric origin, it was suggested [48, 3] that the transition should take place at the same concentration of impurities for any temperature below the Nishimori point, implying verticality of the line. However, recent numerical results for the $\pm J$ RBIM seem to advocate instead a re-entrance of the paramagnetic phase (see Table 1). The other important issue is the nature of the fixed point at zero temperature. It was argued in light of previous numerical results that the universality class of this point could be percolation [17, 25], although there is no obvious reasoning supporting this conclusion in contrast to the case of dilution.

8.1 Flow from the Nishimori point to the pure Ising model

First we study the line which separates the ferromagnetic phase from the paramagnetic phase between the Nishimori point and the pure Ising model. The phase boundary itself has already been determined with good accuracy [19]. Here we will use a computation of the central charge to follow this line in a similar way to what was done in the case of dilution. The motivation for studying this line is first to clearly see in which direction we flow (we expect towards the pure Ising model fixed point since this is a marginally attractive fixed point [1]). Furthermore, we want to check that there is no additional fixed point. In a similar study for the 3-state Potts model [49], an additional fixed point, predicted by perturbation theory [50, 51] was observed.

We start from the pure Ising model, with a small perturbation, say $p = 0.01$ and $T \simeq T_c$, T_c being the critical temperature of the pure Ising model. Next we vary T and measure the central charge. For small p , these measurements are very simple to perform since we have only a weak disorder and moreover, measurements are performed at constant p . It is then easy to determine a maximum since the same configurations of disorder are employed for different T . Then we iterate the process for larger p and follow the ferro-para line which is identified with the maximum of the central charge. The measurement is more complicated close to the Nishimori line because the transition

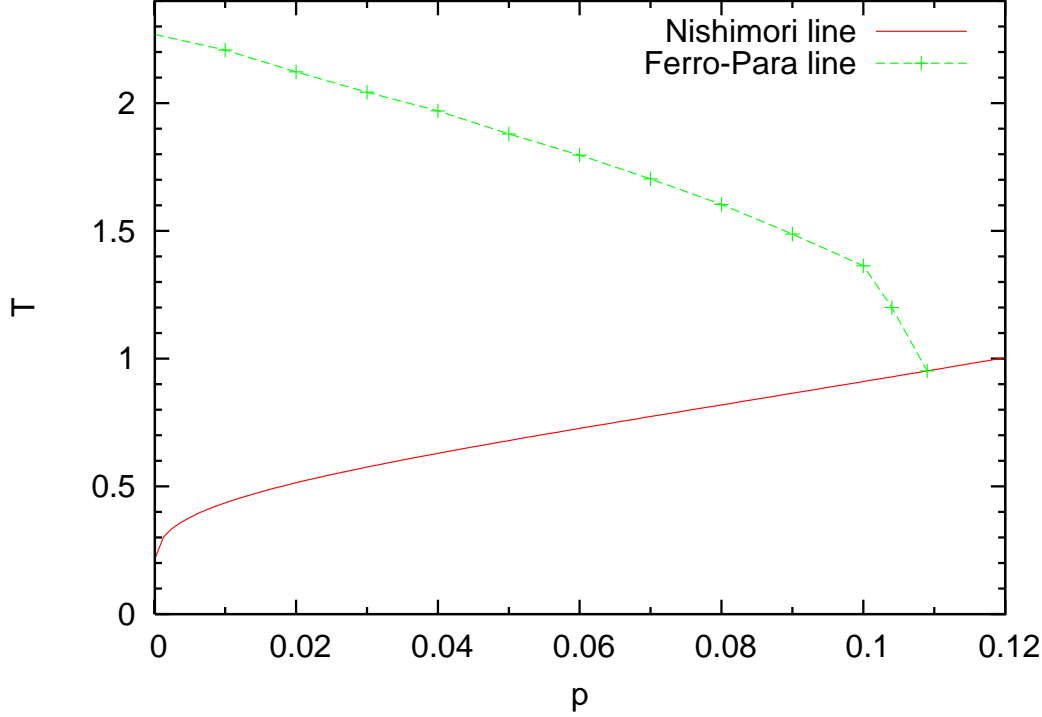


Figure 24: $T - p$ phase diagram for the $J = \pm 1$ disorder case.

line has a strong curvature. One needs to change simultaneously p and T , thus we do not have any more correlated samples and it is much more time consuming to locate the maximum of the central charge (as is the case on the Nishimori line). Fig. 24 shows the phase diagram obtained from the maximum of the central charge. Within error bars, our results agree with the phase diagram Fig. 7 determined in Ref. [19] by a different method. In Fig. 25 we plot the corresponding central charge obtained from three-point fits with $L = 3, 4, 5$ and $L = 4, 5, 6$. Since the difference of the central charge between the pure Ising model and the Nishimori point is very small, we employed a parameter X defined as follows:

$$X = \frac{c_{\text{eff}}(p) - c_{\text{eff}}(p = 0.109)}{c_{\text{eff}}(p = 0) - c_{\text{eff}}(p = 0.109)}, \quad (8.1)$$

similar to the one defined in the study of dilution, see eq. (7.1). From this plot, we can see that by increasing the lattice size, the attractive fixed point is the pure Ising model (since the variation of the central charge increases, starting from the Nishimori point). This is consistent with a flow from the Nishimori point to the pure Ising model and moreover the absence of additional fixed points along this line.

8.2 The zero-temperature fixed point

In this subsection, we study the zero-temperature fixed point. First we present results for the location of the fixed point at $T = 0$. This was already determined with high precision for the $\pm J$ disorder case by Wang et al. [12] and Amoroso and Hartmann [28]. The result

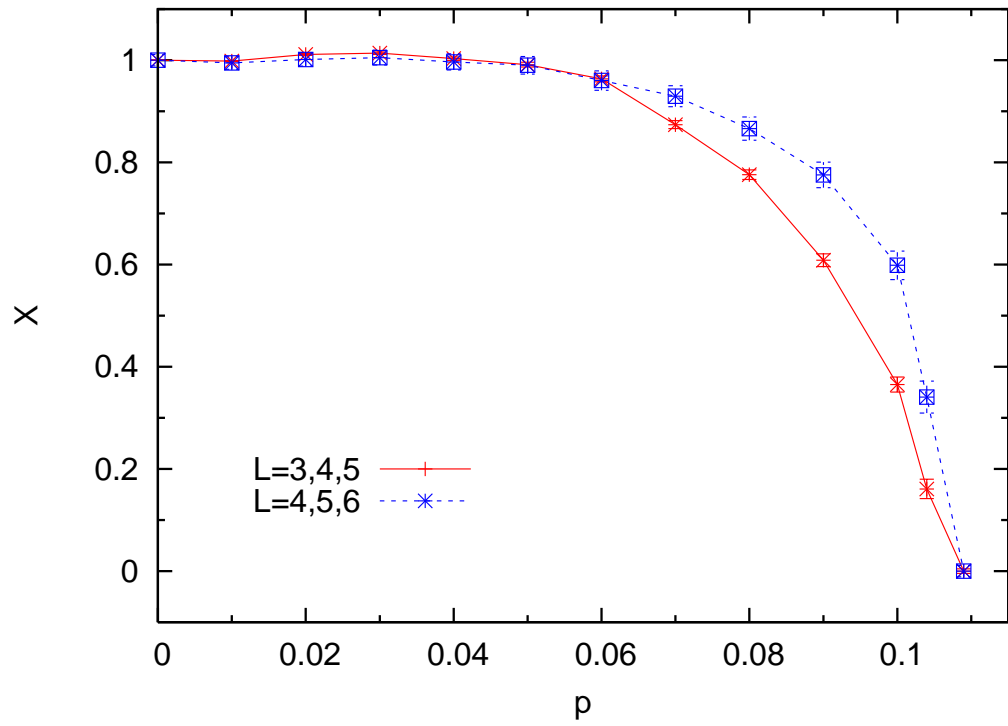


Figure 25: Variation of the effective central charge as characterized by the quantity X (see (8.1)) on the Ferro-Para line, for the $J = \pm 1$ disorder case.

obtained by these groups is $p_c^0 \simeq 0.103$, indicating a re-entrance of the paramagnetic phase. For comparison, we repeated these measurements, obtaining compatible results. We further considered the Gaussian case for which the same re-entrance effect is obtained.

The simulations were performed on square lattices with free boundary conditions along one direction and periodic/antiperiodic conditions in the other direction. We measure the difference of energy between the periodic case and the antiperiodic case

$$\Delta E = E_p - E_a . \quad (8.2)$$

This difference of energy corresponds to the energy associated to a domain wall in the system. We expect that after averaging over disorder, the domain-wall energy is characterized by some size exponent ρ

$$[\Delta E] \propto L^\rho . \quad (8.3)$$

This quantity (as well as the one associated to the width of the distribution of domain-wall energies) was computed with high precision by Amoruso and Hartmann [28] on very large lattices, up to $L = 700$, by using a minimum-weight perfect matching algorithm. In Fig. 26, we present our results on smaller sizes (up to $L = 100$) but with much larger statistics, while employing the same type of algorithm [52]. We simulated 1 million samples for each p and $L < 100$ and 0.5 million samples for $L = 100$, compared to 30 000 samples in [28]. The reason for desiring even better precision is to be able to observe a crossover in the location of the fixed point, see the discussion of this point in the following subsection. In Fig. 26, we clearly distinguish a scaling in function of the size L close to $p \simeq 0.103$ for large L , in perfect agreement with the previous results [12,28]. We also note that this power-law behaviour is apparent only for sizes $L > 20$. In Fig. 27, we present the same quantity for the Gaussian distribution of disorder. Here again we observe a power law of $[\Delta E]$ with size L close to $\sigma \simeq 0.97$ to be compared to the result (3.11) $\sigma_c \simeq 0.97945$ on the Nishimori line. For the Gaussian disorder, we have data up to size $L = 140$ and the number of samples is again 1 million for each value of σ and L except for $L = 140$ where we have 0.5 million samples.

Thus in both cases, we observe a re-entrance of the paramagnetic phase.

8.3 Magnetic exponent at zero temperature

In order to characterize the fixed point at zero temperature we measure the magnetic exponent in the same manner as on the Nishimori line. Specifically, we use measurements of the spin-spin correlation functions which provide a direct estimate of the magnetic exponents and allow us to study higher moments.

Fig. 28 shows the values of η_1 , obtained from the measured spin-spin correlation functions with a fit to the form eq. (5.3). We see in this figure that η_1 is constant close to $p = 0.107 - 0.108$, at least for the largest sizes that we can reach, $L = 20$. For larger sizes, we expect that this value can still decrease, see the discussion below. Next, in Fig. 29, we compare the magnetic exponent (or more precisely $\eta_1 = 2x_h$) obtained for the $\pm J$ distribution of disorder, both on the Nishimori line and at $T = 0$. In this figure, one can see that the critical point at $T = 0$, denoted by p_c^0 is very close to p_c , the critical point on the Nishimori line. The best measurements yields a value of p_c^0 slightly smaller than p_c , close to 0.108. This value is far from the one obtained in the previous section, *i.e.*

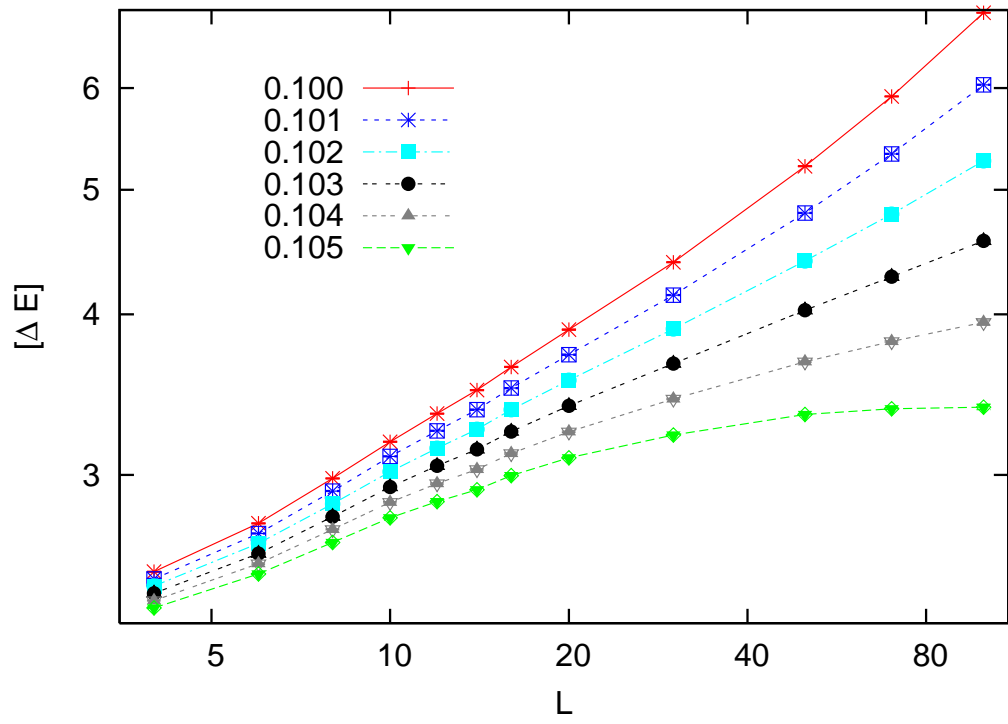


Figure 26: Domain-wall energy $[\Delta E]$ as a function of the system size L for the $\pm J$ disorder at $T = 0$ and for $p = 0.100, \dots, 0.105$.

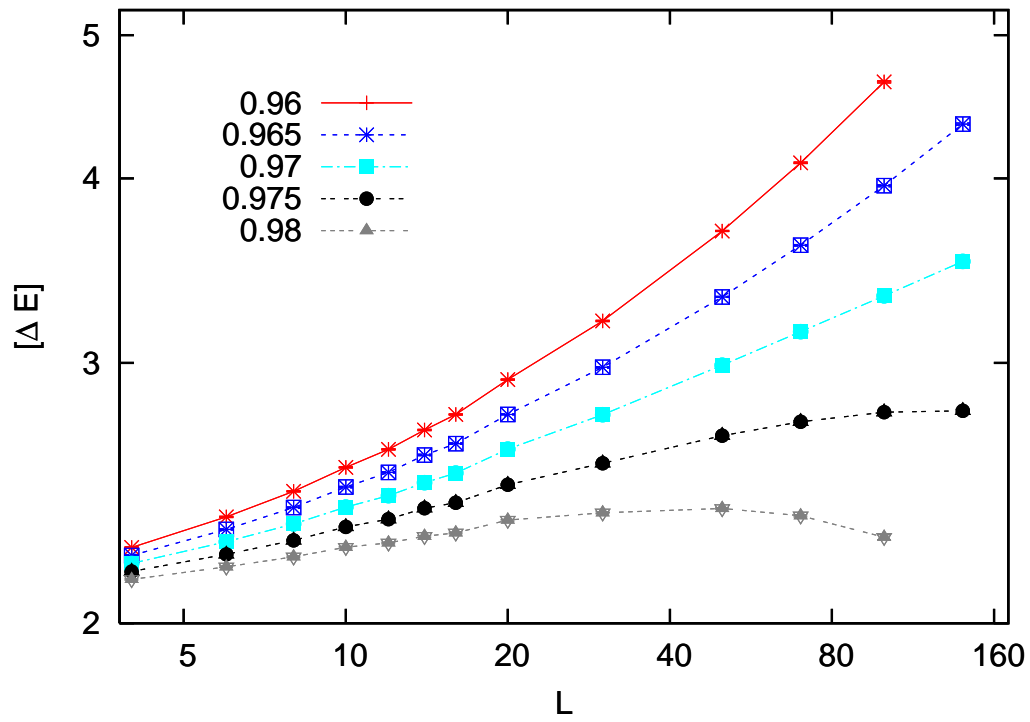


Figure 27: Domain-wall energy $[\Delta E]$ as a function of the system size L for the Gaussian disorder at $T = 0$ and for $\sigma = 0.96, \dots, 0.98$.

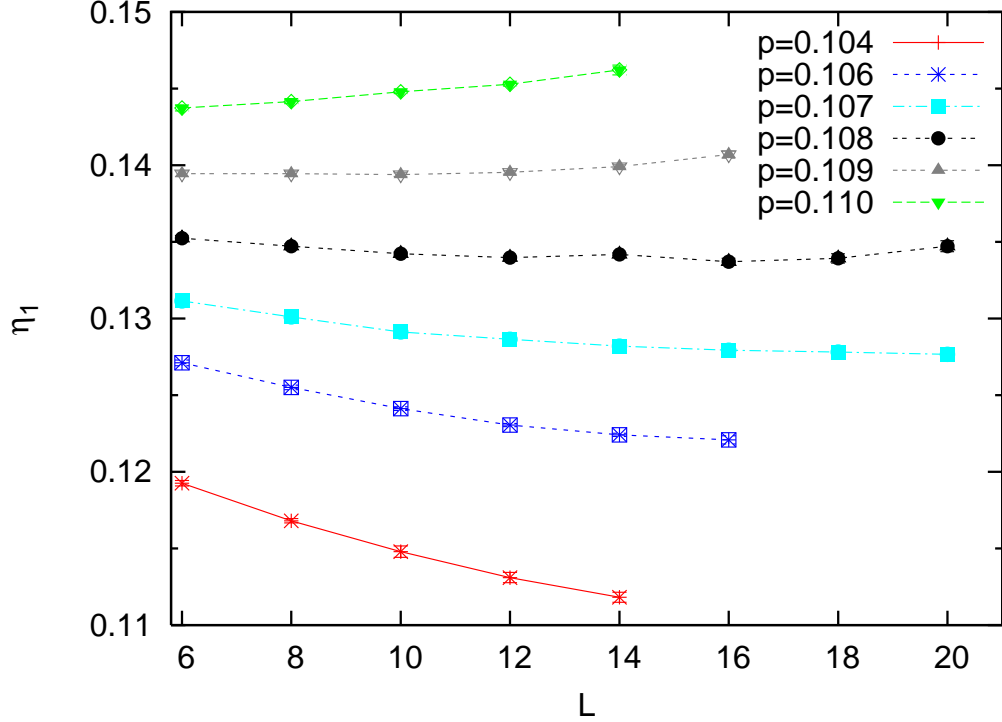


Figure 28: Effective magnetic exponent η_1 vs. L for the $\pm J$ disorder case at $T = 0$.

$p_c^0 = 0.103$. We explain this difference by the existence of strong finite-size corrections, a situation which is frequent for two-dimensional spin glasses, see [53]. These finite-size corrections can also be observed directly in Fig. 28. For small sizes, $6 \leq L \leq 10$, the effective exponent η_1 is constant for $p \simeq 0.109$ and only for this value of p . For $10 \leq L \leq 14$, it is almost constant for $p \simeq 0.108$. By increasing L , the estimate for p_c^0 will continue to decrease. For the largest size that we simulated, p_c^0 is estimated close to 0.107. Presumably, this value will still decrease with increasing size. In the discussion in the previous subsection, we had already observed that a power-law behaviour is apparent only for $L > 20$.

Fig. 30 shows η_1 for the Gaussian distribution of disorder on the Nishimori line and at $T = 0$. Here again, we clearly observe a small re-entrance, with $\sigma_c^0 \simeq 0.97$ compared to $\sigma_c \simeq 0.97945$ (see (3.11)) on the Nishimori line. Contrary to the $\pm J$ disorder case, there are very small finite-size effects. For $L \simeq 14$, one already obtains the same result for σ_c^0 as by domain-wall measurements on much bigger systems.

Finally, let us compare the value of the magnetic exponents for the two types of disorder at $T = 0$. For the Gaussian disorder, one obtains $\eta_1 = 0.11 - 0.12$, see Fig. 30. The $\pm J$ disorder case is less clear. In Fig. 29, as discussed above, one still has strong finite-size corrections. If one considers the asymptotic point $p_c^0 \simeq 0.103$ (compare section 8.2), then the corresponding η_1 will be close to 0.11, thus rather close to the one of the $\pm J$ disorder case. Still, this is not sufficient to conclude that we have universality at $T = 0$. Indeed, at $T = 0$, the type of disorder influences the degeneracy of the ground states. For the Gaussian distribution of disorder, each correlation function (before averaging over

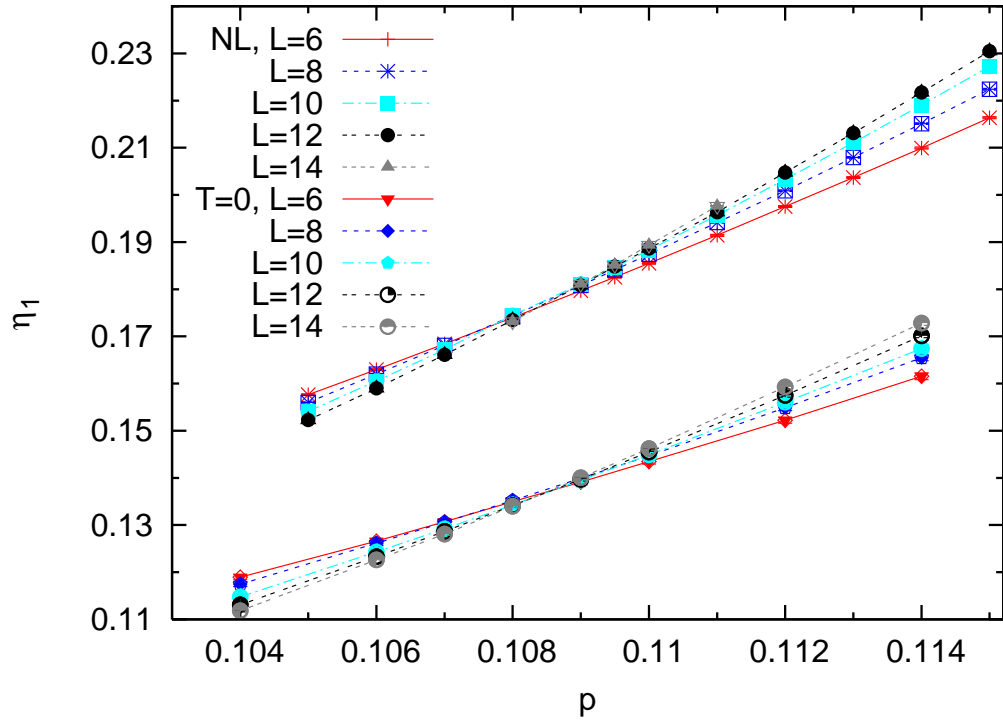


Figure 29: Effective magnetic exponent η_1 vs. p for $\pm J$ disorder case on the Nishimori line and at $T = 0$.

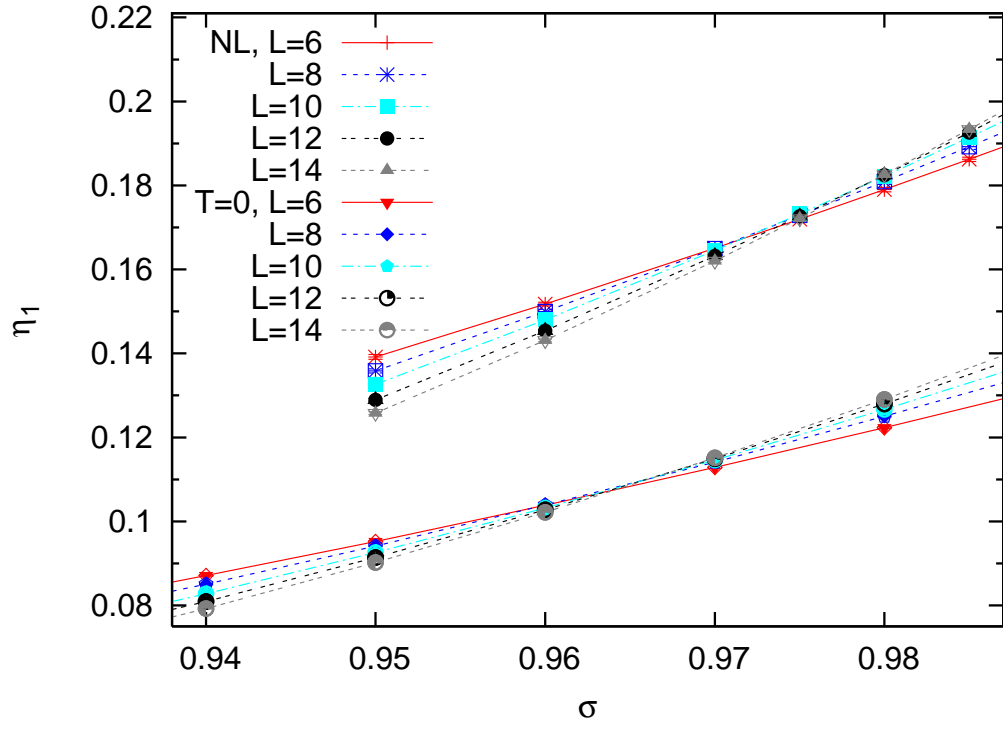


Figure 30: Effective magnetic exponent η_1 vs. σ for Gaussian disorder on the Nishimori line and at $T = 0$.

disorder) will be equal to ± 1 . Thus the even moments will always be equal to one, while the odd moments will be equal to the first moment. Then, one obtains the general result, valid as long the ground state is unique (up to a global symmetry), $\eta_{2n+1} = \eta_1$ for any n and $\eta_{2n} = 0$. On the contrary, for the $\pm J$ disorder case, we have a huge degeneracy of the ground states. A direct determination of the exponents η_i for $L = 20$ and $p = 0.107$ yields:

$$\begin{aligned}\eta_1 &= 0.1277 \pm 0.0004 & ; & \quad \eta_2 = 0.0593 \pm 0.0002 \\ \eta_3 &= 0.1369 \pm 0.0004 & ; & \quad \eta_4 = 0.0719 \pm 0.0002 \\ \eta_5 &= 0.1412 \pm 0.0004 & ; & \quad \eta_6 = 0.0776 \pm 0.0002 \\ \eta_7 &= 0.1438 \pm 0.0004 & ; & \quad \eta_8 = 0.0810 \pm 0.0002.\end{aligned}\tag{8.4}$$

The value $p = 0.107$ is chosen even if it is not exactly at the asymptotic critical point $p_c^0 \simeq 0.103$ since for this value we have measurements for large sizes. We also computed the same exponents for smaller p and smaller L . The change in the exponents is very small. We thus conclude that for the $\pm J$ disorder case, all moments are different.

9 Summary and conclusions

In this paper we have performed an extensive study of the random-bond Ising model with a particular emphasis on non-trivial fixed points. Concerning the Nishimori point, which is located at the intersection of the Ferro-Para critical line and the Nishimori line, we have used domain-wall free energy computations to provide an accurate estimate for the location of this multicritical point. This has been done for both, the binary $\pm J$ distribution as well as for the Gaussian distribution. Our numerical results show that a conjecture for the location of the Nishimori point based on a duality argument [21] yields only a very good approximation, but is not exact.

Next, we estimated $\nu = 1.48(3)$ for $\pm J$ disorder and $\nu = 1.52(3)$ for Gaussian disorder. This agrees with other recent estimates for $\pm J$ disorder, namely $\nu = 1.50(3)$ on the square lattice [19], and $\nu = 1.49(2)$ on the triangular and honeycomb lattices [54]. All these results are consistent with a universal value $\nu \approx 1.50$ for the Nishimori point. We have obtained further accurate results for the exponents η_1, \dots, η_8 for the moments of the spin-spin correlation functions. The estimates for $\pm J$ disorder (5.6) and Gaussian disorder (5.7) are not only very close to each other, but also to recent estimates on the triangular and honeycomb lattices [54]. Our analysis of the central charge c at the Nishimori point for both types of disorder is also consistent with a universal value $c = 0.464 \pm 0.004$ [15]. All these results⁶ suggest a single universality class of the Nishimori point in the two-dimensional random-bond Ising model, and definitely exclude percolation as the possible universality class for this point.

We have also considered a probability distribution for the bonds with dilution, in which some of the coupling constants are zero. In the purely diluted case (a distribution containing only positive or zero bonds) there is only one non-trivial fixed point,

⁶Essentially the same results are found [55] if the approximate value $p_c \approx 0.110028$ [21] is used instead of the numerically exact value (3.4).

namely the zero-temperature percolation point, apart from the critical point of the pure system [36]. We have confirmed that this percolation point is unstable against the Nishimori point if one moves within the intersection of the critical transition surface and the Nishimori manifold by considering both, dilution and $\pm J$ couplings, and that these two points (percolation and Nishimori) are the only fixed points within this intersection line. On the other hand, going off the Nishimori line but staying within the critical transition line we confirm that the Nishimori point is unstable in favour the pure Ising model fixed point. All these results are obtained by studying the crossover of the effective central charge, or first Lyapunov exponent, in strips of increasing width.

Finally, we have analyzed the critical point at zero temperature corresponding to the ferro-para transition in the model without dilution for both the binary and Gaussian distributions. Our numerical analysis confirms the strict re-entrance of the ferromagnetic phase [12, 28]. We have also investigated the criticality of the zero-temperature fixed point and argued that it is, as for the finite-temperature Nishimori point, different from percolation. The results obtained in this paper raise the question of the apparent hierarchy of fixed points for strongly disordered systems, namely in our case the pure Ising transition, percolation, the Nishimori point and the zero-temperature point, all corresponding to different (and certainly non-unitary) conformal field theories with values for the central charge and critical exponents which are extremely close to each other but nevertheless different. Future analytical efforts will be needed to understand such effects of strong disorder in two-dimensional classical statistical systems.

References

- [1] Vik. S. Dotsenko and Vl. S. Dotsenko, *Sov. Phys. JETP Lett.* **33** (1981) 37; *Adv. Phys.* **32** (1983) 129; B. N. Shalaev, *Sov. Phys. Solid State* **26** (1984) 1811; A. W. Ludwig, *Nucl. Phys. B* **330** (1990) 639
- [2] H. Nishimori, *J. Phys. C: Solid State Phys.* **13** (1980) 4071; *Prog. Theor. Phys.* **66** (1981) 1169
- [3] Y. Ozeki and H. Nishimori, *J. Phys. A: Math. Gen.* **26** (1993) 3399
- [4] A. Georges and P. Le Doussal, *unpublished Preprint* (1988); P. Le Doussal and A. B. Harris, *Phys. Rev. Lett.* **61** (1988) 625; *Phys. Rev. B* **40** (1989) 9249
- [5] S. Cho and M. P. A. Fisher, *Phys. Rev. B* **55** (1997) 1025
- [6] I. A. Gruzberg, N. Read and A. W. W. Ludwig, *Phys. Rev. B* **63** (2001) 104422
- [7] J. T. Chalker, N. Read, V. Kagalovsky, B. Horovitz, Y. Avishai and A. W. Ludwig *Phys. Rev. B* **65** (2001) 012506
- [8] A. Mildenberger, F. Evers, R. Narayanan, A. D. Mirlin and K. Damle, *Phys. Rev. B* **73** (2006) 121301(R)
- [9] N. Sourlas, *Europhys. Lett.* **25** (1994) 159; *Preprint cond-mat/9811406*
- [10] H. Nishimori, *Physica A* **205** (1994) 1; *Physica A* **315** (2002) 243

- [11] Y. Iba, *J. Phys. A: Math. Gen.* **32** (1999) 3875
- [12] C. Wang, J. Harrington and J. Preskill, *Annals Phys.* **303** (2003) 31
- [13] M. R. Zirnbauer, *J. Math. Phys.* **37** (1996) 4986; A. Altland and M. R. Zirnbauer, *Phys. Rev. B* **55** (1997) 1142
- [14] I. A. Gruzberg, N. Read and A. W. W. Ludwig, *Phys. Rev. Lett.* **82** (1999) 4524; J. Cardy, *Phys. Rev. Lett.* **84** (2000) 3507
- [15] A. Honecker, M. Picco and P. Pujol, *Phys. Rev. Lett.* **87** (2001) 047201
- [16] W. L. McMillan, *Phys. Rev. B* **29** (1984) 4026
- [17] R. R. P. Singh and J. Adler, *Phys. Rev. B* **54** (1996) 364
- [18] F. D. A. Araújo Reis, S. L. A. de Queiroz and R. R. dos Santos, *Phys. Rev. B* **60** (1999) 6740
- [19] F. Merz and J. T. Chalker, *Phys. Rev. B* **65** (2002) 054425
- [20] F. Merz and J. T. Chalker, *Phys. Rev. B* **66** (2002) 054413
- [21] H. Nishimori and K. Nemoto, *J. Phys. Soc. Jpn.* **71** (2002) 1198; H. Nishimori, *Preprint cond-mat/0602453*
- [22] G. Grinstein, C. Jayaprakash and M. Wortis, *Phys. Rev. B* **19** (1979) 260
- [23] H. Freund and P. Grassberger, *J. Phys. A: Math. Gen.* **22** (1989) 4045
- [24] J. Bendish, U. Derigs and A. Metz, *Discrete Applied Mathematics* **52** (1994) 139
- [25] N. Kawashima and H. Rieger, *Europhys. Lett.* **39** (1997) 85
- [26] G. Migliorini and A. N. Berker, *Phys. Rev. B* **58** (1998) 426
- [27] J. A. Blackman, J. R. Gonçalves and J. Poulter, *Phys. Rev. E* **58** (1998) 1502
- [28] C. Amoruso and A. K. Hartmann, *Phys. Rev. B* **70** (2004) 134425
- [29] C. M. Newman and D. L. Stein, *Phys. Rev. Lett.* **84** (2000) 3966; *Commun. Math. Phys.* **224** (2001) 205
- [30] Y. Ozeki and H. Nishimori, *J. Phys. Soc. Jpn.* **56** (1987) 3265
- [31] Y. Ozeki and N. Ito, *J. Phys. A: Math. Gen.* **31** (1998) 5451
- [32] J. M. Maillard, K. Nemoto and H. Nishimori, *J. Phys. A: Math. Gen.* **36** (2003) 9799
- [33] G. Mussardo and P. Simonetti, *Phys. Lett. B* **351** (1995) 515
- [34] D. C. Cabra, A. Honecker, G. Mussardo and P. Pujol, *J. Phys. A: Math. Gen.* **30** (1997) 8415

- [35] M. P. Nightingale, pp. 287-351 in: V. Privman (ed.), *Finite Size Scaling and Numerical Simulations of Statistical Physics*, World Scientific, Singapore (1990)
- [36] J. M. Yeomans and R. B. Stinchcombe, *J. Phys. C: Solid State Phys.* **12** (1979) 347
- [37] D. Stauffer and A. Aharony, *Introduction to Percolation Theory*, 2nd edition, Taylor & Francis, London (1994)
- [38] E. S. Sørensen, *Preprint* cond-mat/0006233
- [39] A. Honecker, J. L. Jacobsen, M. Picco and P. Pujol, *Statistical Field Theories*, Como, 18-23 June 2001, eds. A. Cappelli, G. Mussardo, Kluwer Academic Publishers, Dordrecht (2002) 251-261 [*Preprint* cond-mat/0112069].
- [40] H. W. J. Blöte, J. L. Cardy and M. P. Nightingale, *Phys. Rev. Lett.* **56** (1986) 742; I. Affleck, *Phys. Rev. Lett.* **56** (1986) 746
- [41] J. L. Jacobsen and J. L. Cardy, *Nucl. Phys. B* **515** (1998) 701
- [42] J. Cardy, *Scaling and Renormalization in Statistical Physics*, Cambridge Lecture Notes in Physics 5, Cambridge University Press (1996)
- [43] K. G. Wilson and J. Kogut, *Phys. Rep.* **12** (1974) 75
- [44] S. L. A. de Queiroz and R. B. Stinchcombe, *Phys. Rev. B* **68** (2003) 144414
- [45] J. L. Cardy, in *Phase Transitions and Critical Phenomena*, Vol. 11, edited by C. Domb and J. Lebowitz, Academic Press, London (1987)
- [46] K. Binder, *Z. Phys. B* **43** (1981) 119
- [47] D. P. Landau and K. Binder, *A Guide to Monte Carlo Simulations in Statistical Physics*, Cambridge University Press (2000)
- [48] H. Nishimori, *J. Phys. Soc. Jpn.* **55** (1986) 3305; H. Kitatani, *J. Phys. Soc. Jpn.* **61** (1992) 4049
- [49] J. L. Jacobsen and M. Picco, *Phys. Rev. E* **65** (2002) 026113
- [50] A. W. W. Ludwig, *Nucl. Phys. B* **285** (1987) 97
- [51] V. Dotsenko, M. Picco and P. Pujol, *Nucl. Phys. B* **455** (1995) 701
- [52] W. Cook and A. Rohe, *INFORMS Journal on Computing* **11** (1999) 138
- [53] A. K. Hartmann and M. A. Moore, *Phys. Rev. Lett.* **90** (2003) 127201
- [54] S. L. A. de Queiroz, *Phys. Rev. B* **73** (2006) 064410
- [55] J. C. Lessa and S. L. A. de Queiroz, *Preprint* cond-mat/0605659